Probing shell evolution with large-scale shell-model calculations

Yutaka Utsuno

Advanced Science Research Center, Japan Atomic Energy Agency

Center for Nuclear Study, University of Tokyo

Nuclear-structure approaches

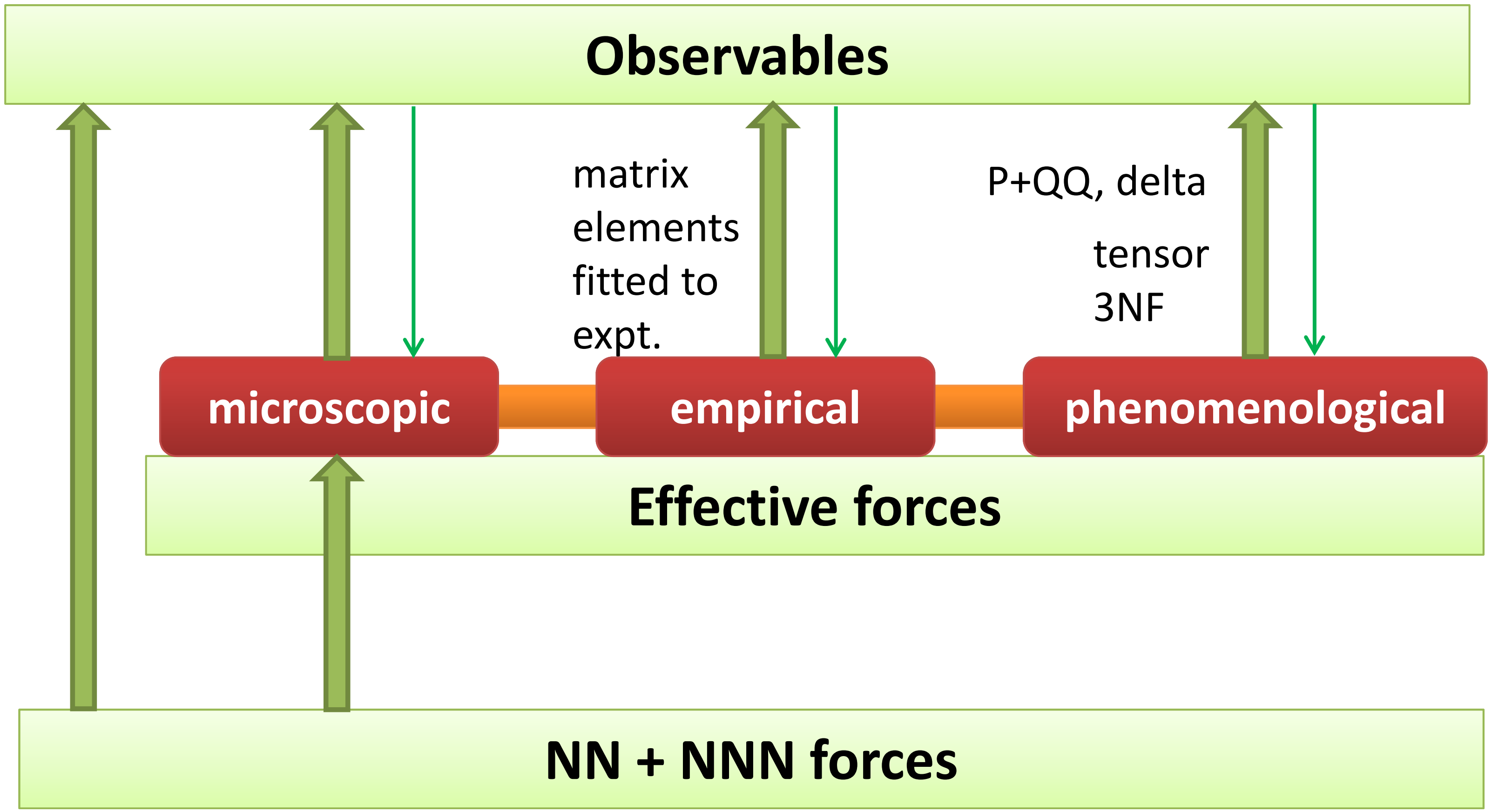

- Mutual communication among microscopic, empirical, and phenomenological approaches becomes important.

Monopole matrix elements: case of *pf*-shell

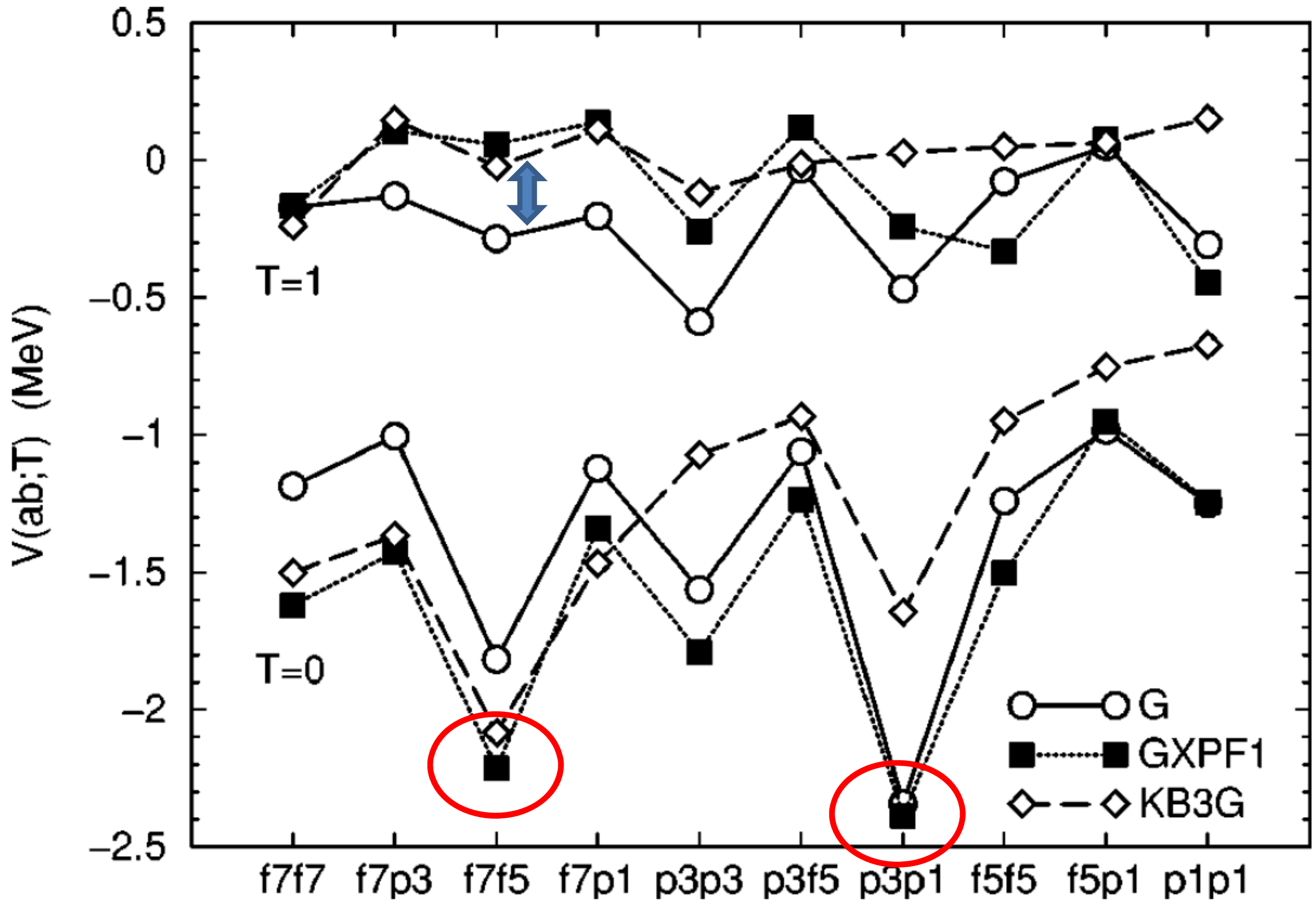

M. Honma et al., Phys. Rev. C 69, 034335 (2004)

- Strong $j_{>}$-$j'_{<}$ attraction particularly for the T=0 channel: tensor
- Empirical interaction: overall repulsive shift for the T=1 monopole

Monopole-based universal interaction V_{MU}

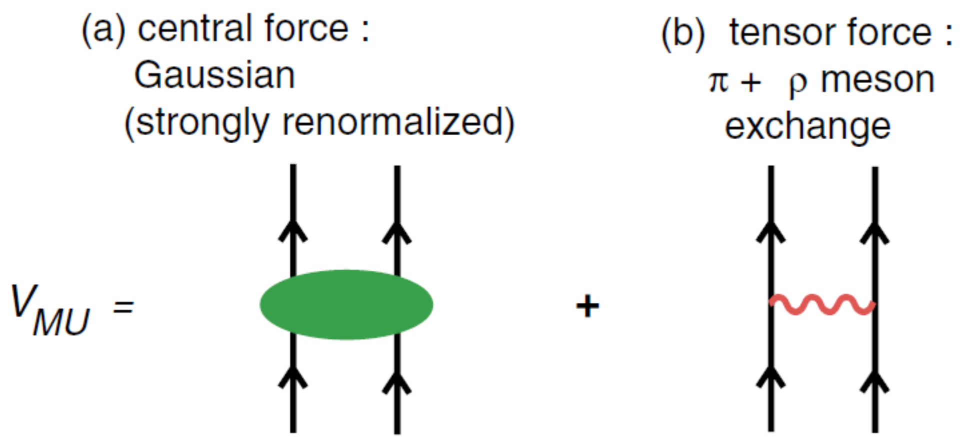

T. Otsuka et al., Phys. Rev. Lett. 104, 012501 (2010).

- Bare tensor
  - Renormalization persistency
- Phenomenological Gaussian central
  - Supported by empirical interactions

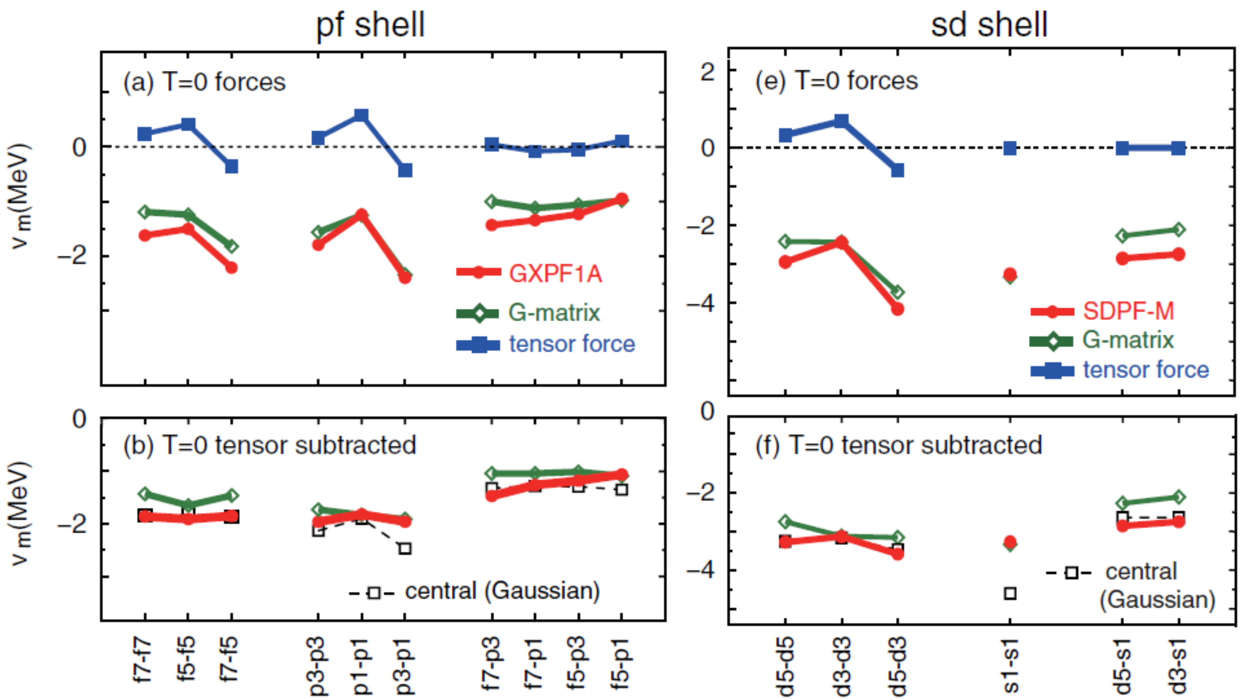

Effect of three-nucleon forces

- Contributing to repulsion in T=1 two-body forces
- Ab-initio-type calculations give similar effects.
- V_{MU} includes this effect implicitly.

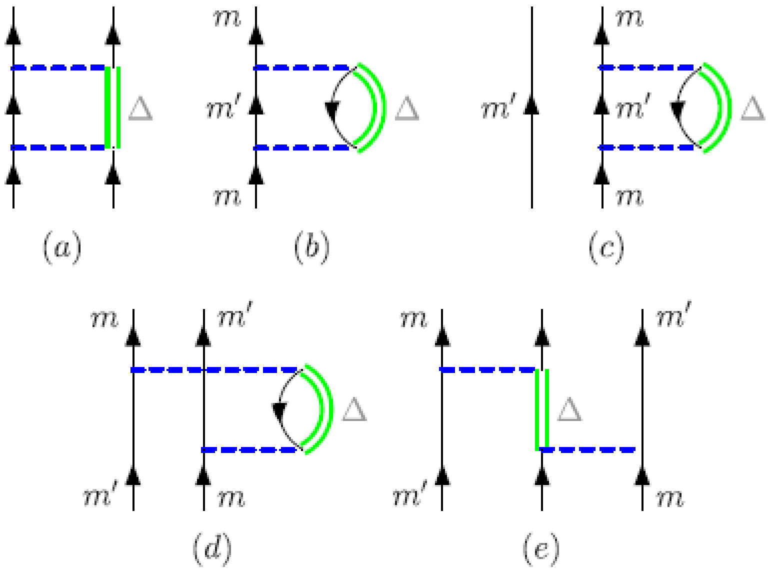

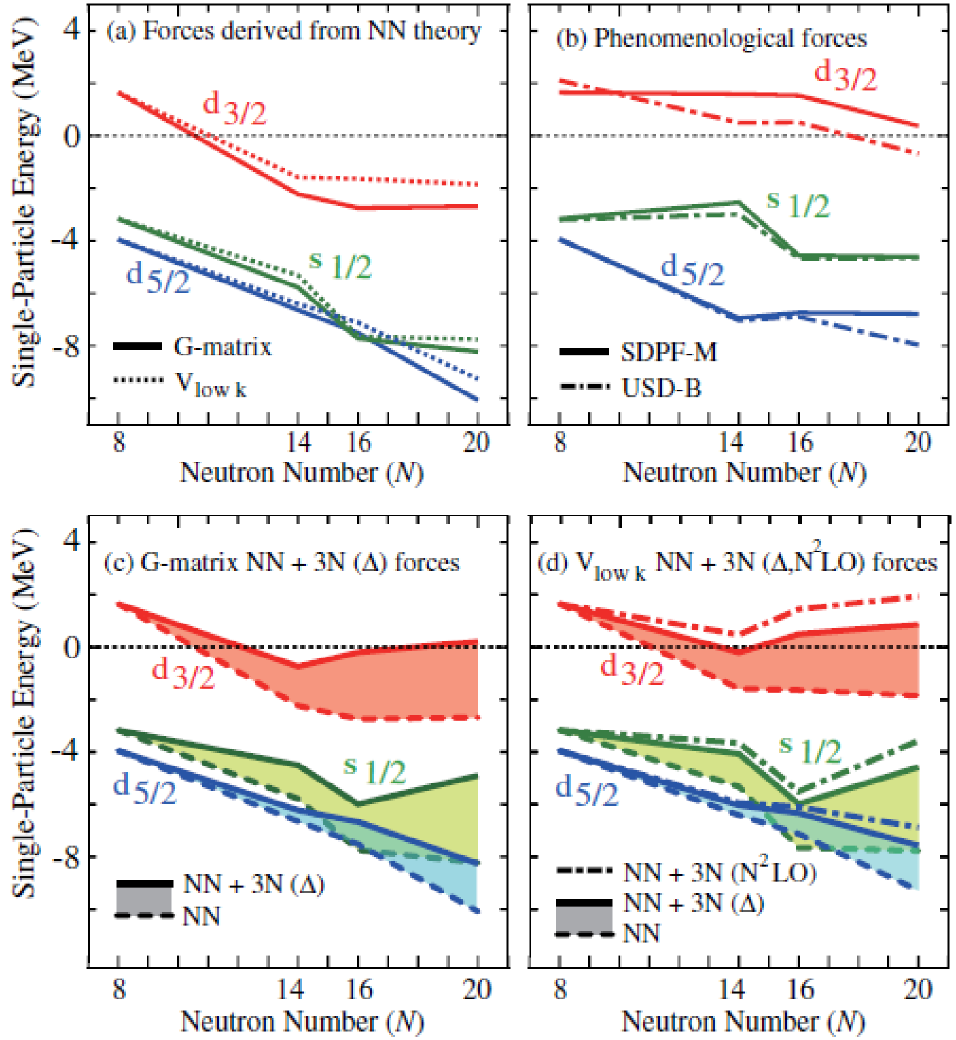

T. Otsuka et al., Phys. Rev. Lett. 105, 032501 (2010).

Outline of this talk

- Shell-model calculations using V_{MU} combined with empirical interactions

1. Shell evolution caused by T=1 monopole interactions
    1. Unnatural-parity states of neutron-rich Si isotopes (very briefly)
    2. Unnatural-parity states of neutron-rich Cr-Ni isotopes
    3. Unnatural-parity states of neutron-rich Ca isotopes
2. Application of large-scale shell-model calculation to photonuclear reactions
    – Ca isotopes
3. Analyzing shell-model wave functions in terms of mean-field picture
    – Origin of the exotic isomeric 4^+ state in ^{44}S

Collaborators

- V_{MU}: T. Otsuka, T. Suzuki, M. Honma, K. Tsukiyama, N. Tsunoda, M. Hjorth-Jensen
- sd-pf: T. Otsuka, B. A. Brown, M. Honma, T. Mizusaki, N. Shimizu
- Cr-Ni: T. Togashi, N. Shimizu, T. Otsuka, M. Honma
- Ca: T. Otsuka, N. Shimizu, M. Honma, T. Mizusaki
- E1: N. Shimizu, T. Otsuka, S. Ebata, M. Honma
- ^{44}S: N. Shimizu, T. Otsuka, T. Yoshida, Y. Tsunoda

Refined V_{MU} for the shell-model

- tensor: $\pi+\rho$
- spin-orbit: M3Y
  - Works in some cases
- central: to be close to GXPF1
  - Including "density dependence" to better fit empirical interactions

a good guide for a shell-model interaction without direct fitting to experiment

Central force fitted with six parameters

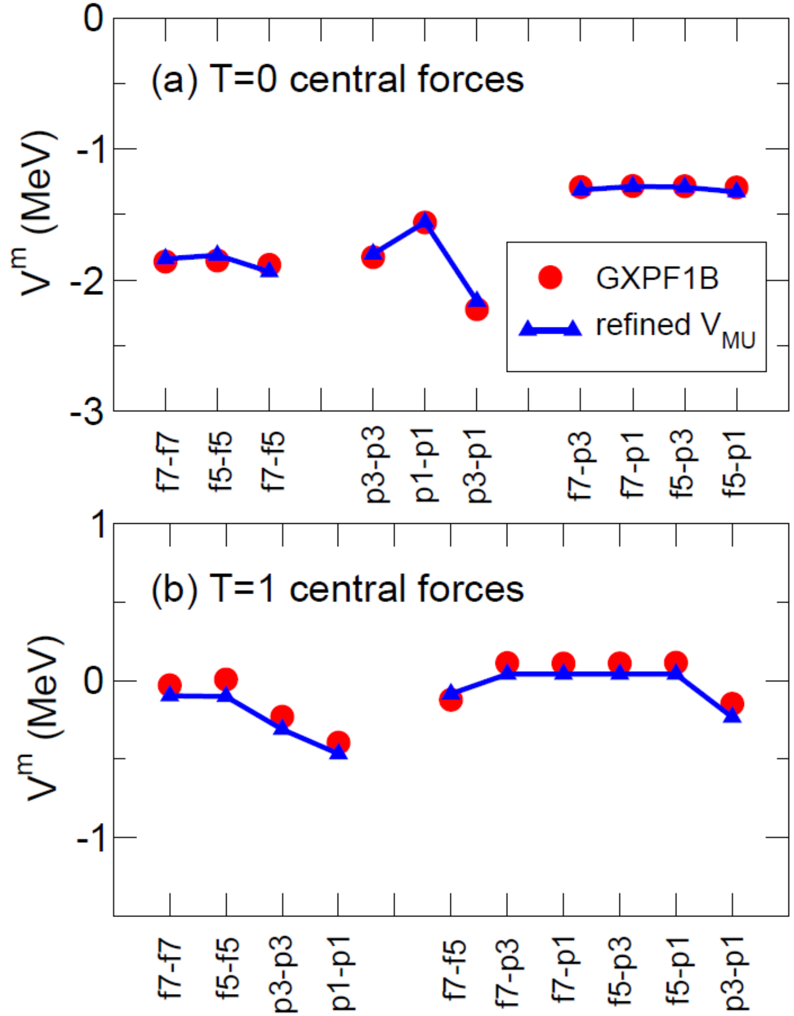

Y. Utsuno et al., EPJ Web of Conferences 66, 02106 (2014).

T=1 monopole: case of *sd*-*pf* shell

- SDPF-MU interaction based on the refined V_{MU}
  - USD for the *sd* shell and GXPF1B for the *pf* shell
  - Refined V_{MU} for the cross-shell

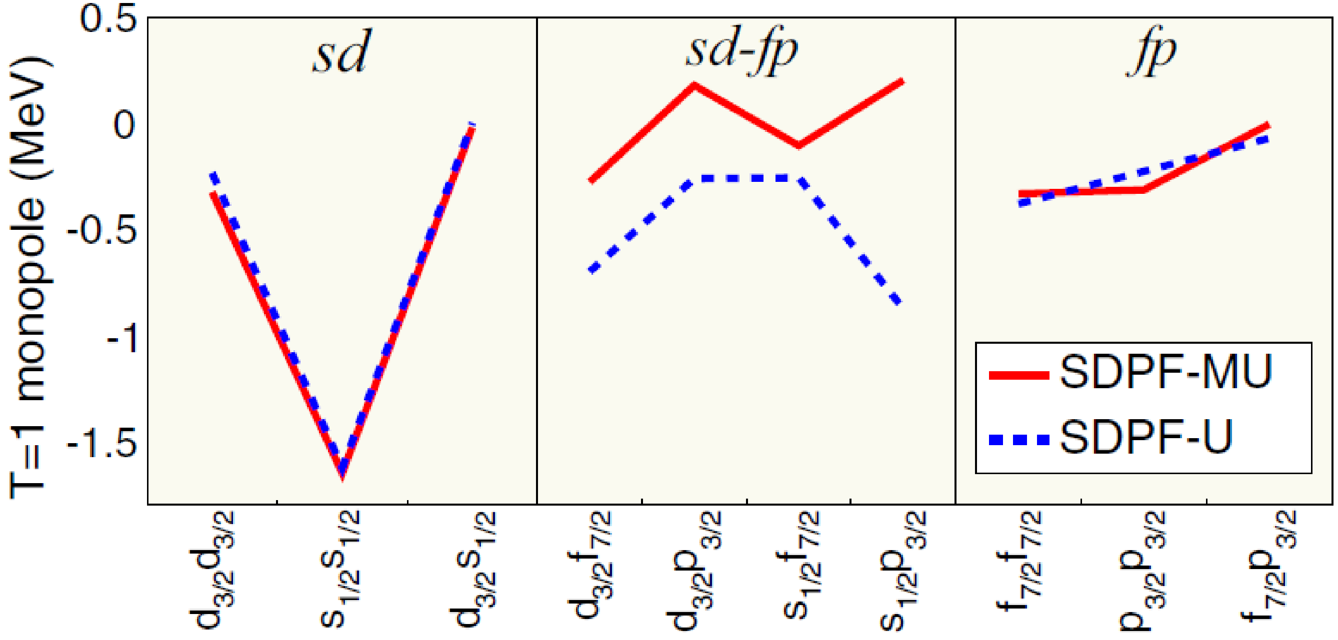

S. R. Stroberg, A. Gade et al., Phys. Rev. C 91, 041302(R) (2015).

Cross-shell of SDPF-U: two-body G martix

Evolution of unnatural-parity states in Si

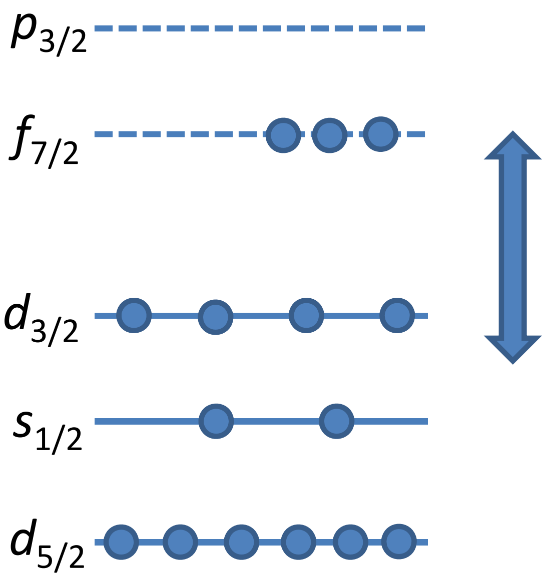

The gap changes with increasing neutrons in $f_{7/2}$ depending on the T=1 monopole strength.

Unnatural-parity states are good indicators of the gap.

- A recent experiment at NSCL supports nearly zero value of T=1 cross-shell monopole matrix elements.

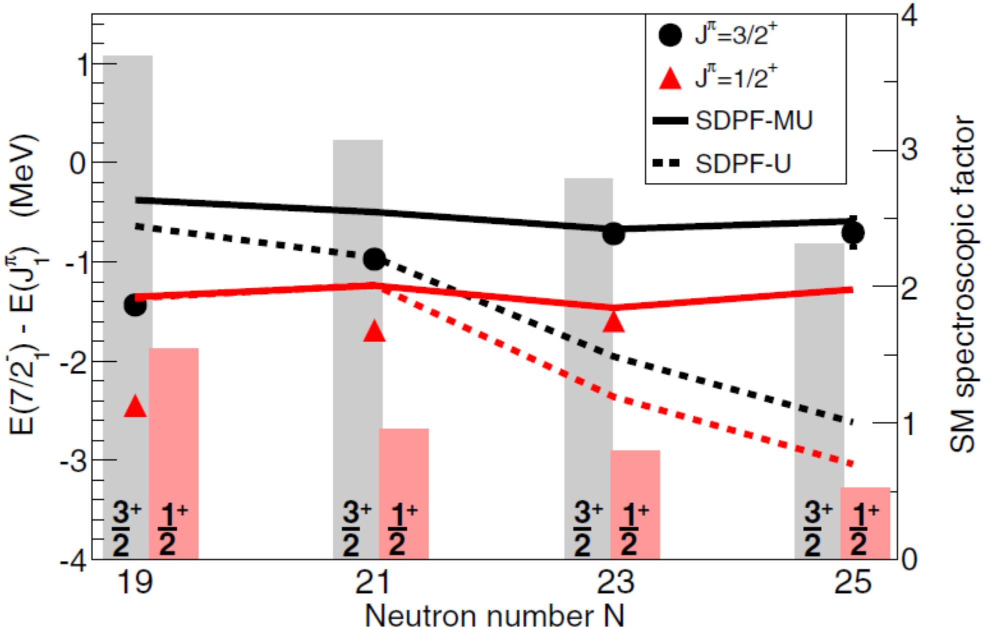

S. R. Stroberg, A. Gade et al., Phys. Rev. C 91, 041302(R) (2015).

Sharp drop of the 9/2$^+$ level in Cr, Fe and Ni

Experimental 9/2$^+$ levels in Cr, Fe, and Ni isotopes

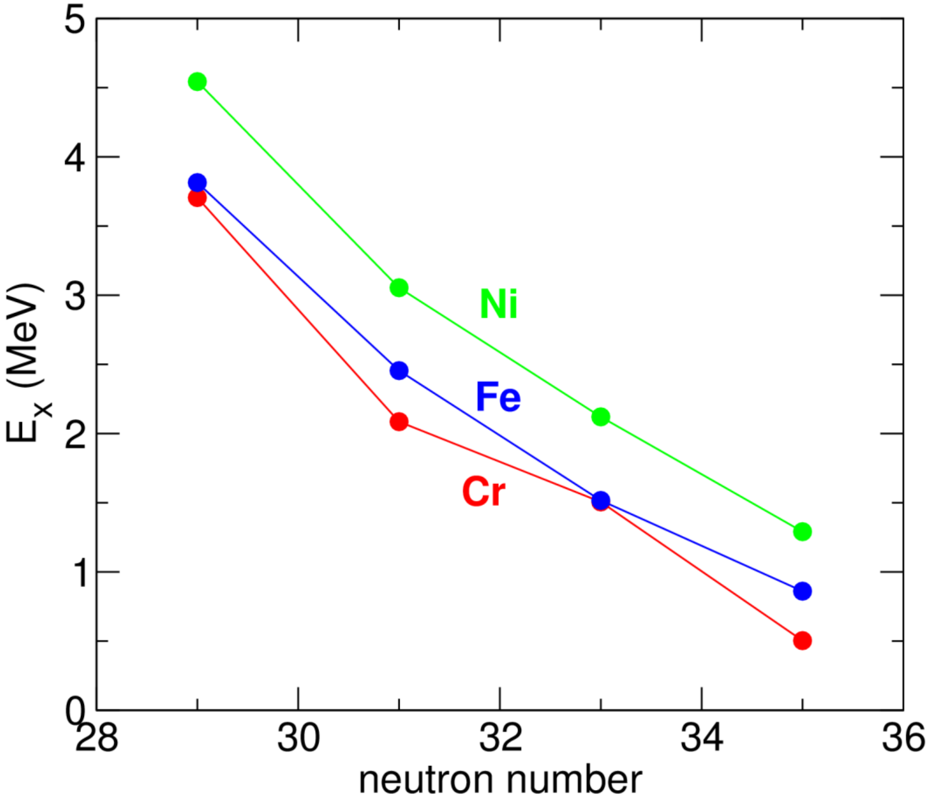

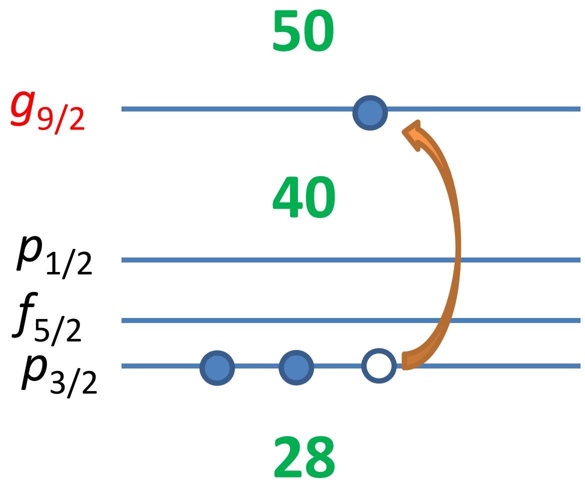

- Does this mean the reduction of the N=40 gap due to the T=1 monopole interaction?

Shell-model calculation

T. Togashi et al., Phys. Rev. C 91, 024320 (2015).

- Model space
  - Valence shell: full *pf* shell + $0g_{9/2}$ + $0d_{5/2}$
  - Allowing up to one neutron excitation from the *pf* shell to the upper orbits
    - $N \leq 35$ isotopes are *pf*-shell nuclei
    - One can use an empirical *pf*-shell interaction as it is because of no coupling to 2p-2h or 3p-3h configurations.
  - *M*-scheme dimension: up to 1.8×10^{10} for ^{59}Ni (manageable with KSHELL)
- Effective interaction
  - GXPF1Br for the *fp* shell + the refined V_{MU}
  - One modification for $\langle g_{9/2} f_{5/2} | V | g_{9/2} f_{5/2}; J, T = 1 \rangle$
  - SPE of $g_{9/2}$ (one free parameter): determined to fit the overall $9/2^+$ levels
  - SPE of $d_{5/2}$: not sensitive to the results; effective gap from $g_{9/2} \approx 2$ MeV

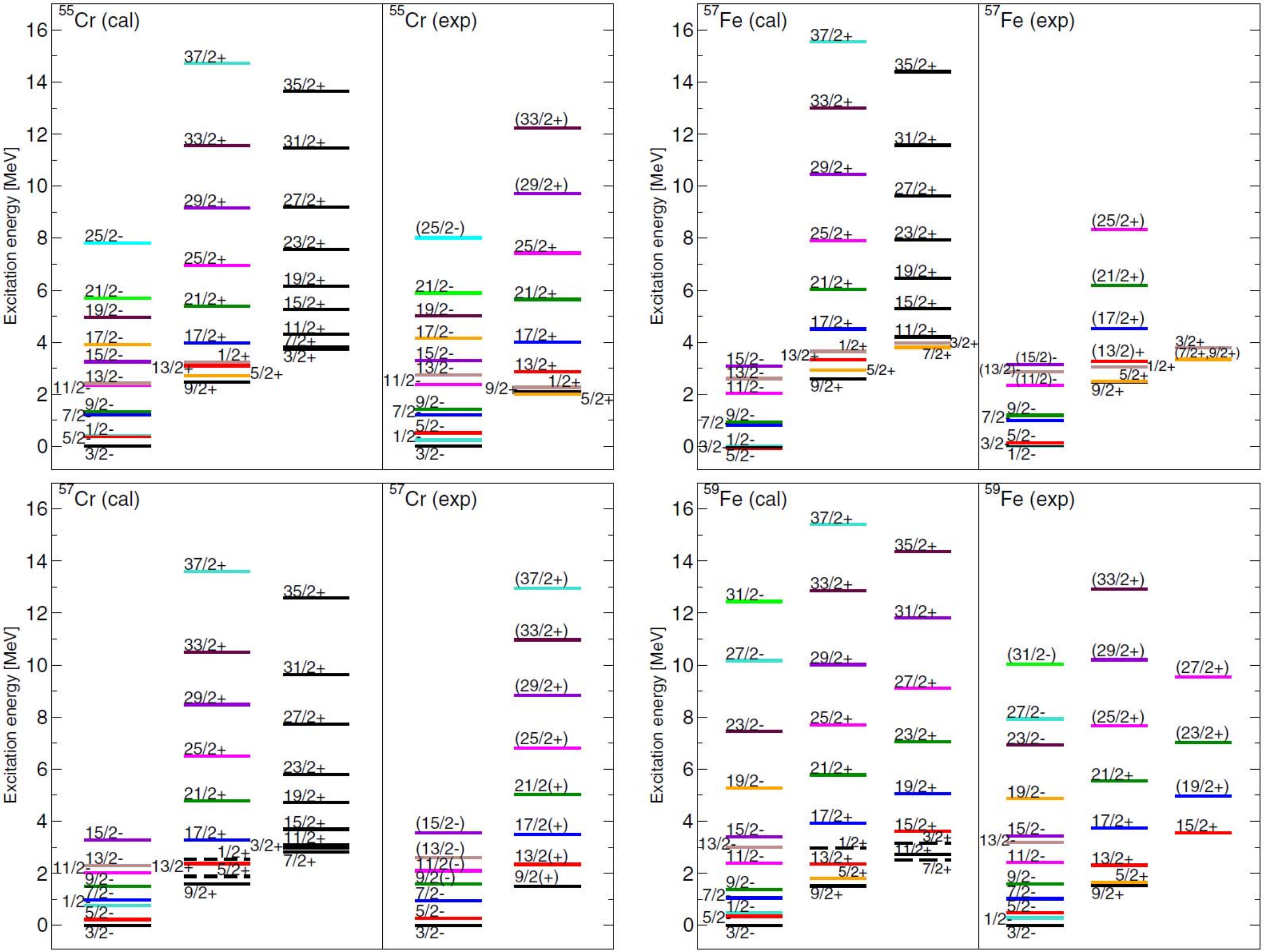

Good agreement including unfavored-signature states

Evolution of the 9/2$^+$ levels

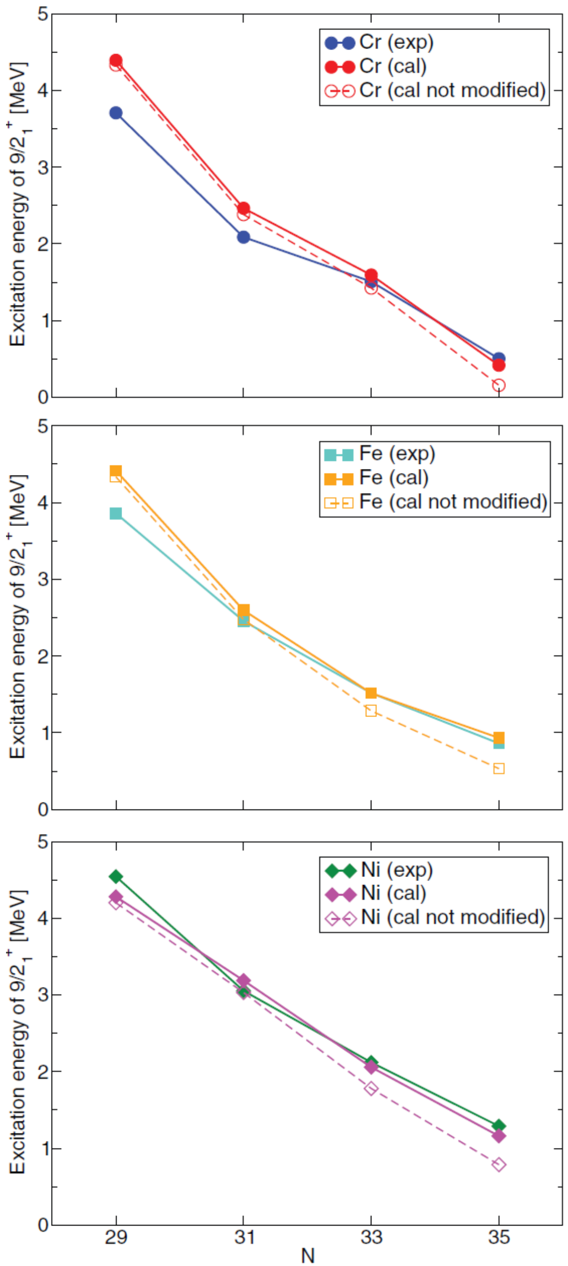

	Cal	Exp
	$C^2S\,(9/2_1^+)$	
^{53}Cr	0.564	0.520 [65], 0.95 [66], 0.57 [67]
^{55}Cr	0.458	0.67 [66], 0.582 [68]
^{57}Cr	0.479	–
^{59}Cr	0.498	–
^{55}Fe	0.568	0.74 [69], 0.465 [70], 0.375 [85], 0.67 [86]
^{57}Fe	0.494	0.270 [71], 0.447 [72]
^{59}Fe	0.442	0.510 [73], 0.38 [74]
^{61}Fe	0.527	–
^{57}Ni	0.611	–
^{59}Ni	0.580	0.84 [75], 0.47 [76], 0.56 [74], 0.381 [77], 0.390 [85], 0.69 [87]
^{61}Ni	0.503	0.62 [78], 0.750 [79], 0.8450 [80], 0.537 [81]
^{63}Ni	0.446	0.61 [69], 0.672 [82], 0.75 [83], 0.75 [84]

- Positions and spectroscopic strengths are well reproduced.
  - Large single-neutron amplitudes for the 9/2$^+$

Evolution of the $g_{9/2}$ orbit

- $g_{9/2}$ and $d_{5/2}$ orbits are kept almost constant with *N*.
  - Due to nearly zero *T*=1 cross-shell monopole matrix elements according to V_{MU}
- Simple estimate of the location of $g_{9/2}$ from measurement
  - Binding energy of the $9/2^+$ level measured from the even-*N* core $= -S_n + E_x(9/2^+)$
  - Nearly constant with *N* both from experiment and calculation

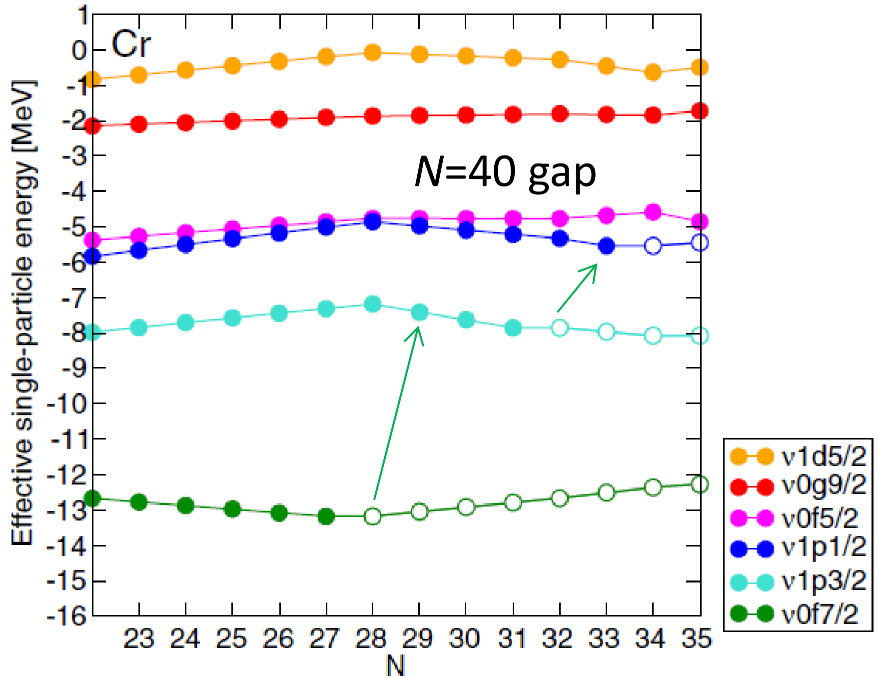

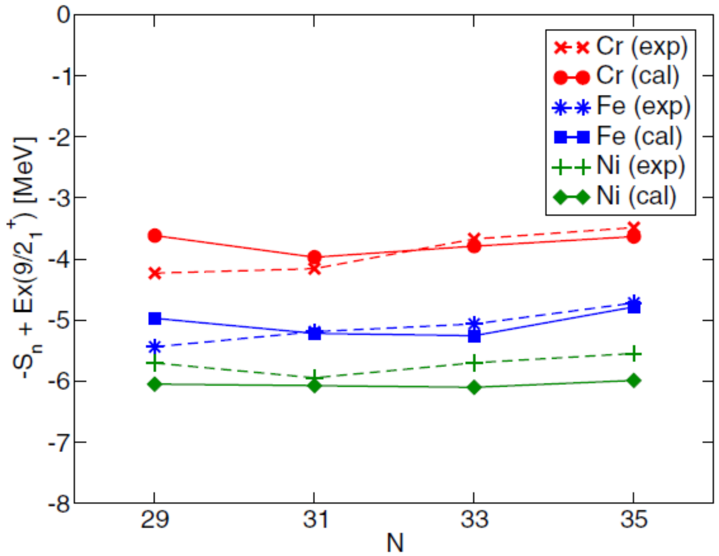

Investigating $g_{9/2}$ in *n*-rich Ca isotopes

- $g_{9/2}$ orbit in neutron-rich Ca isotopes
  - Plays a crucial in determining the drip line and the double magicity in ^{60}Ca
- What is learned from the study of Cr-Ni isotopes
  - The $g_{9/2}$ orbit does not change sharply at least for $N \leq 35$ isotopes.
  - Similar evolution should occur in Ca isotopes, too.
- How to spot the position of $g_{9/2}$ in Ca isotopes?
  - Unnatural-parity states: similar to Cr-Ni cases
  - One should also take into account excitation from the *sd* shell to the *pf* shell: not dominant in Cr-Ni region

Shell-model calculation

- Model space
  - Full *sd*-*pf*-*sdg* shell
  - Allowing one nucleon excitation from the *sd* shell to the *pf* shell or the *pf* shell to the *sdg* shell: full $1\hbar\omega$ calculation

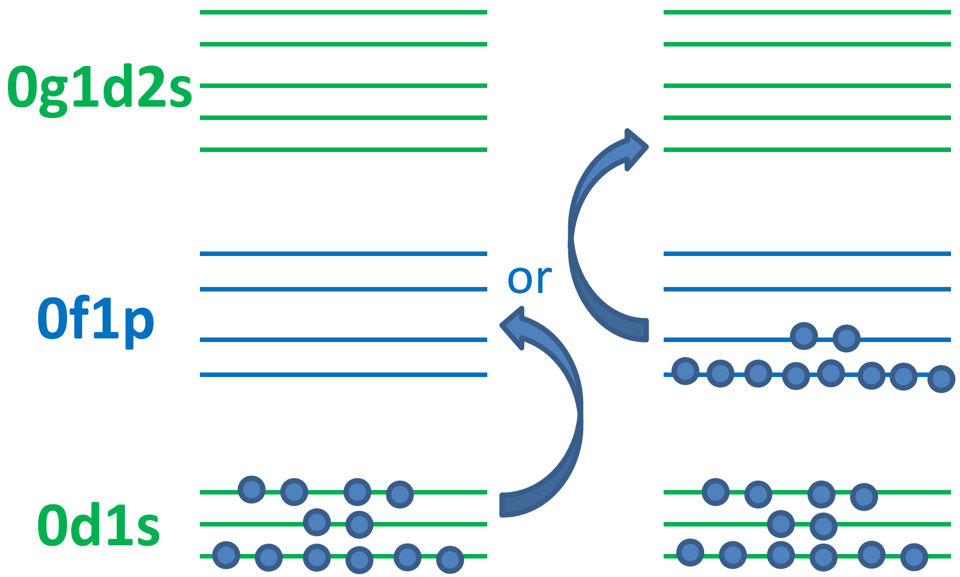

- Effective interaction
  - A natural extension of SDPF-MU and the one used for Cr-Ni isotopes: SDPF-MU for the *sd*-*pf* shell + the refined V_{MU} for the other
    - SDPF-MU: USD (*sd*) + GXPF1B (*pf*) + the refined V_{MU} for the other
  - SPE of $g_{9/2}$: needed to refit because of activating excitation from *sd* to *pf* → determined to fit the $9/2^{+}_{1}$ level in ^{50}Ti (C^2S = 0.37 or 0.54)
  - SPE of other *sdg* orbits: to follow schematic Nilsson SPE

Systematics of the 3^-_1 state in even-*A* Ca

- Three calculations
  - A) excitations from *sd* to *pf* only
  - B) excitations from *pf* to *sdg* only
  - C) full $1\hbar\omega$ configurations
- 3^-_1 levels
  - – *sd-pf* calc.
    - good agreement for $N \leq 28$
    - large deviation for $N > 28$
  - – full $1\hbar\omega$ calc.
    - Strong mixing with the *sdg* configuration accounts for the stable positioning of the 3^- levels.

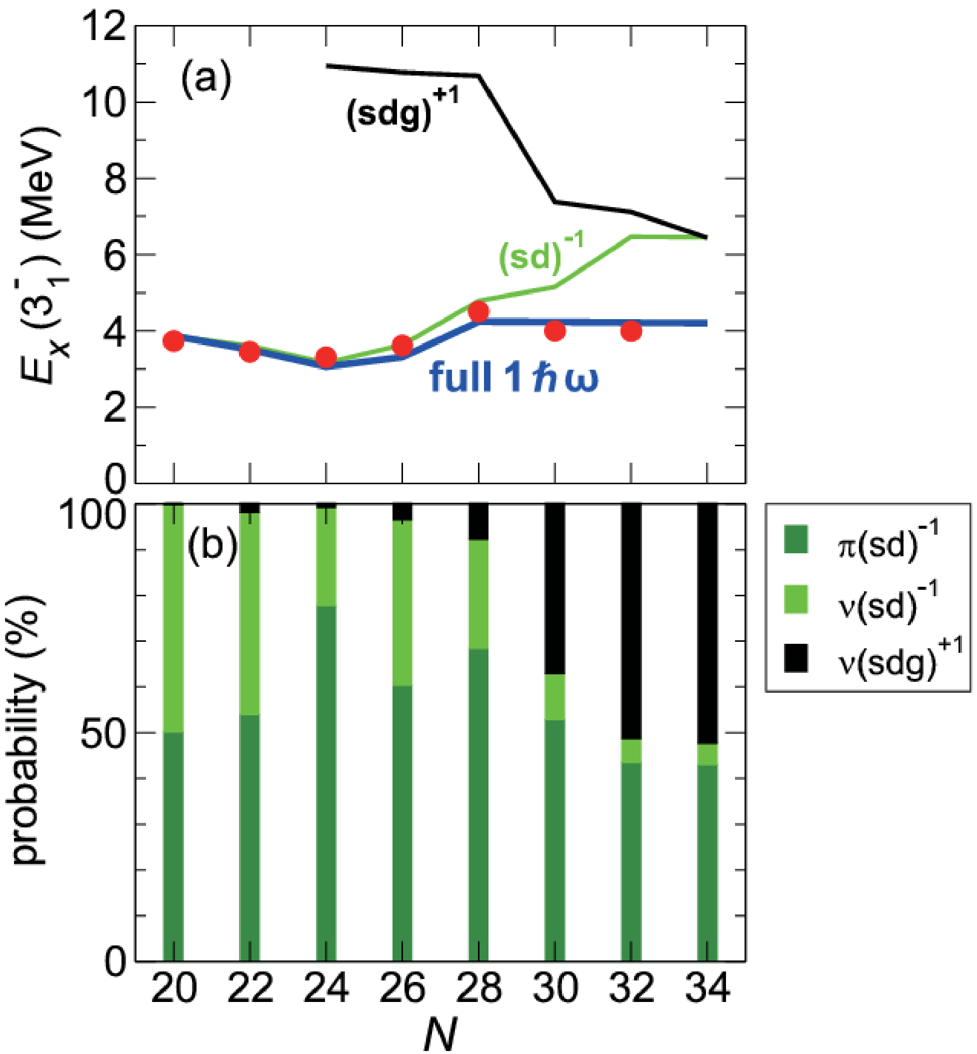

3^-_1 configuration probed by direct reaction

- ^{50}Ca: strongly populated by the ^{48}Ca(*t*, *p*) reaction
  - **neutron** excitation

Relative ^{48}Ca(t, p) maximum cross section

State	Energy (MeV)	θ (angle in c.m. system)	$\frac{d\sigma(\theta)}{d\Omega}$ (exp)	$\frac{d\sigma(\theta)}{d\Omega}$ (th. $\varepsilon^2 = 0$)	$\frac{d\sigma(\theta)}{d\Omega}$ (th. $\varepsilon^2 = 0.02$)
g.s.	0	5°	100	100	100
2_1^+	1.03	20°	42	39	32
2_2^+	3.00	20°	36	40	36
0_2^+	3.53	5°	2	5.5	2.4
(3^-)	3.99	28°	21	43	37
0_3^+	4.47	5°	2.2	1.0	0.5

R. A. Broglia et al., Nucl. Phys. A 106, 421 (1968).

- ^{52}Ca: strongly populated by the 2*p* knockout from ^{54}Ti
  - **proton** excitation

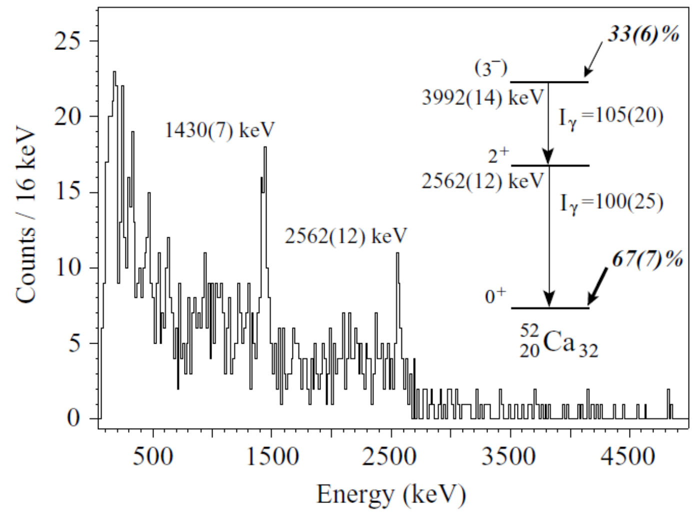

A. Gade et al., Phys. Rev. C 74, 021302(R) (2006).

Without the strong mixing between proton and neutron excitations these properties are hard to explain because larger-*N* nuclei should be more easily excited to higher orbits.

Energy levels of ^{49}Ca

- ^{48}Ca + *n* system
  - Single-particle structure may appear.
  - Core-coupled states can compete in high excitation energies
- $9/2^+$ state at 4.017 MeV
  - Firm spin-parity assignment made recently (D. Montanani et al., PLB 697, 288 (2011); PRC 85, 044301 (2012).)
    - interpreted as core-coupled state
  - Present calc.: Strong mixing with $g_{9/2}$ is also important.
    - Good B(E3)

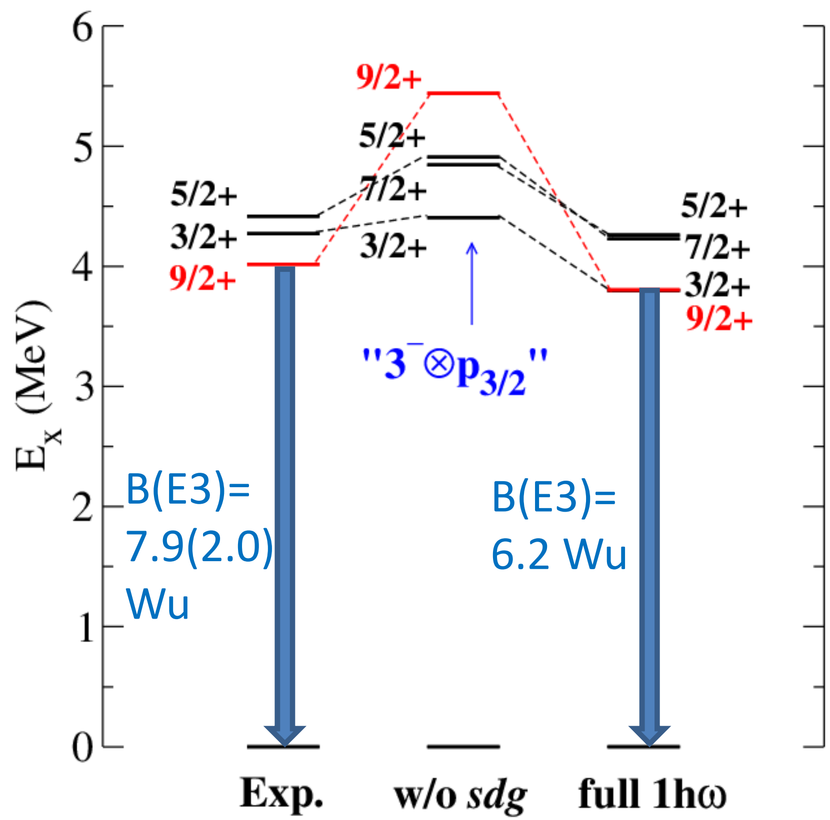

	$3/2^+_1$	$5/2^+_1$	$7/2^+_1$	$9/2^+_1$
% of *sdg*	6	9	7	**51**

Systematics of $g_{9/2}$ strength in N=29 isotones

	dimension	E_x (MeV)		C^2S (n attached)	
		Expt.	Calc.	Expt.	Calc.
^{49}Ca	2,515,437	4.02	3.80	0.14	0.42
^{51}Ti	187,386,759	3.77	3.77	0.37	0.47
^{53}Cr	3,411,147,908	3.71	4.04	0.52	0.47

- 9/2$^+$ of N=29 isotones
  - Shell-model calc. is possible up to ^{53}Cr.
  - Strong mixing with $g_{9/2}$ for all the isotones in calc. but small C^2S for ^{49}Ca in expt.
    - Effect of the doublet? (see right)

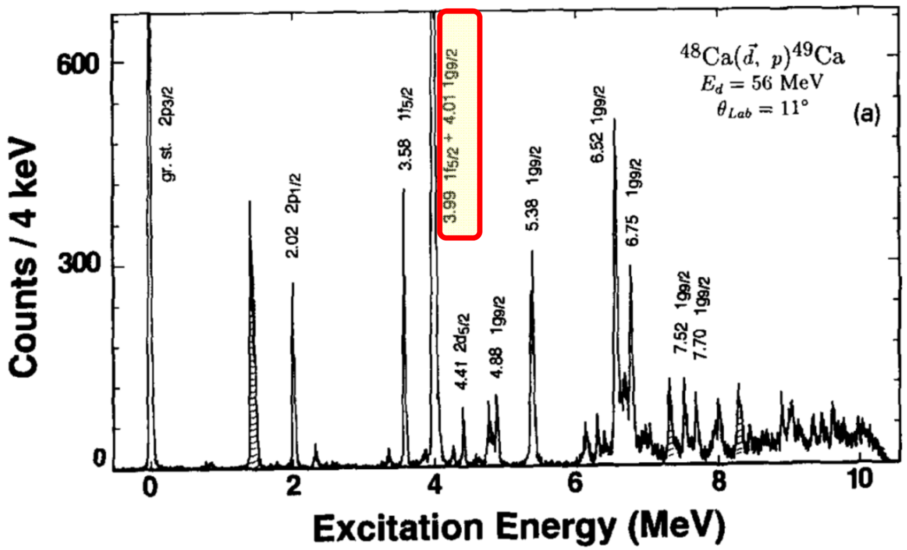

Y. Uozumi et al., Nucl. Phys. A 576, 123 (1994).

Systematics of the $9/2^+_1$ state in odd-A Ca

- $9/2^+_1$ in the *sd-pf* calculation
  - Core-coupled state
  - Located stably at 5-6 MeV
- $9/2^+_1$ in the *pf-sdg* calculation
  - Sharply decreasing due to the shift of the Fermi level
- $9/2^+_1$ in the full $1\hbar\omega$ calculation
  - 3-4 MeV up to *N*=33 but drops considerably at *N*=35
    - Different from Cr-Ni
  - The state at *N*=55 is nearly a single-particle character.
    - Interesting to observe at FRIB

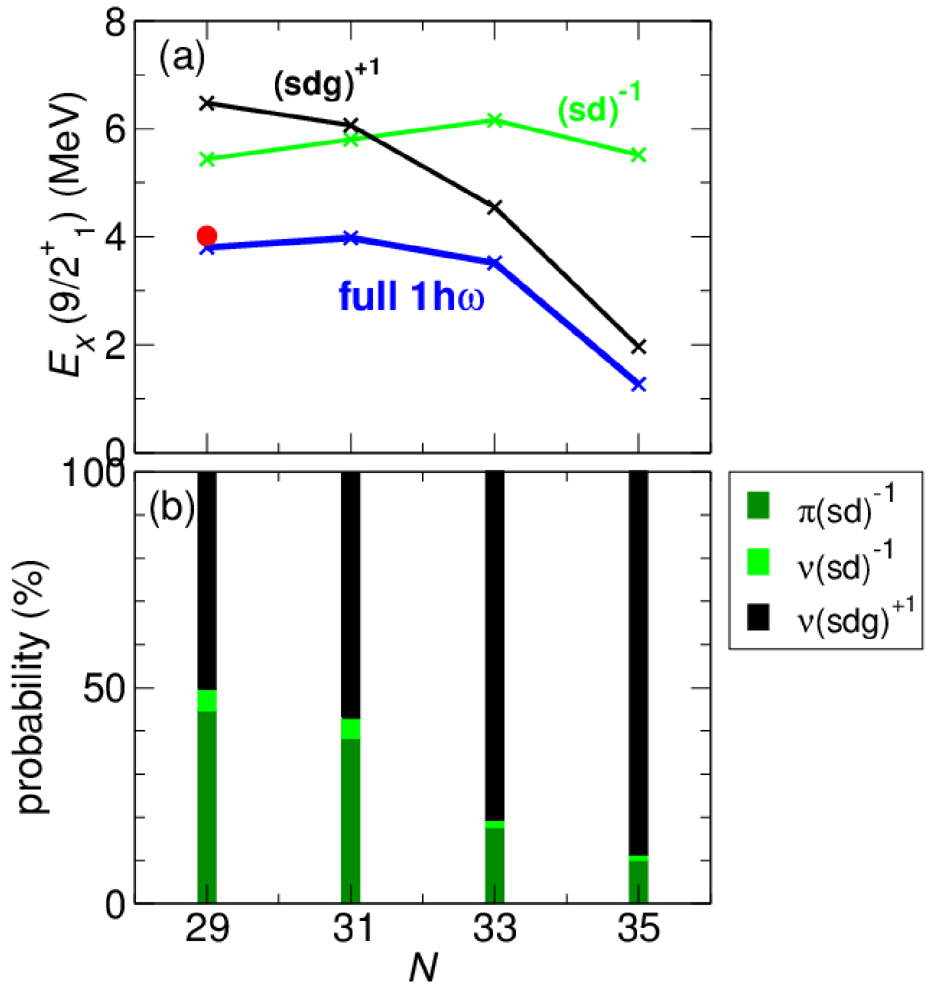

Neutron effective single-particle energy

- Global behavior
  - Stable due to very weak T=1 monopole matrix elements
- Location of $g_{9/2}$
  - 2-3 MeV higher than $f_{5/2}$
  - Whether ^{60}Ca is a good doubly magic nucleus depends on the evolution of $f_{5/2}$ in going from N=34 to 40, which is dominated by the T=1 $f_{5/2}$-$f_{5/2}$ monopole interaction.
    - Is there experimental data that can constrain this monopole?

Ca isotopes

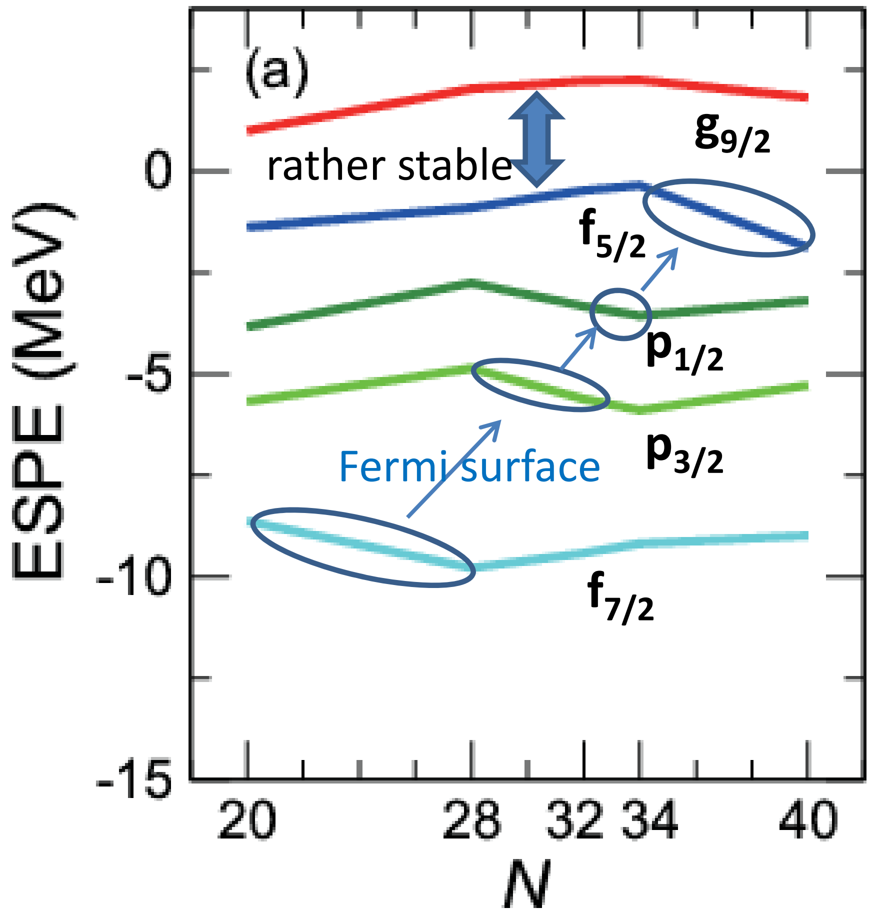

Application to photonuclear reaction

N. Shimizu et al., in preparation

- A good Hamiltonian for the full $1\hbar\omega$ space is constructed.
- It is expected that photonuclear reaction, dominated by $E1$ excitation, is well described with this shell-model calculation:

$$\sigma_{\text{abs}}(E) = \frac{16\pi^3 E}{9\hbar c} S_{E1}(E)$$

with $S_{E1}(E) = \sum_\nu B(E1; g.s. \to \nu)\delta(E - E_\nu + E_0)$

- Shell-model calculation provides good level density, including non-collective levels, the coupling to which leads to the width of GDR.
- Application of shell model to photonuclear reaction has been very limited due to computational difficulty.
  - Sagawa and Suzuki (O isotopes), Brown (^{208}Pb)

Lanczos strength function method

- It is almost impossible to calculate all the eigenstates concerned using the exact diagonalization.
- Moment method of Whitehead [Phys. Lett. B 89, 313 (1980)]
  - The shape of the strength function can be obtained with much less Lanczos iterations.
    1. Take an initial vector: $\overrightarrow{v_1} = T(E1)|\mathrm{g.s.}\rangle$
    2. Follow the usual Lanczos procedure
    3. Calculate the strength function $\sum_\nu B(E1; g.s. \to \nu)\frac{1}{\pi}\frac{\Gamma/2}{(E-E_\nu+E_0)^2+(\Gamma/2)^2}$ by summing up all the eigenstates ν in the Krylov subspace with an appropriate smoothing factor Γ until good convergence is achieved.
  - See Caurier et al., Rev. Mod. Phys. 77, 427 (2005), for application to Gamow-Teller.

Convergence of strength distribution

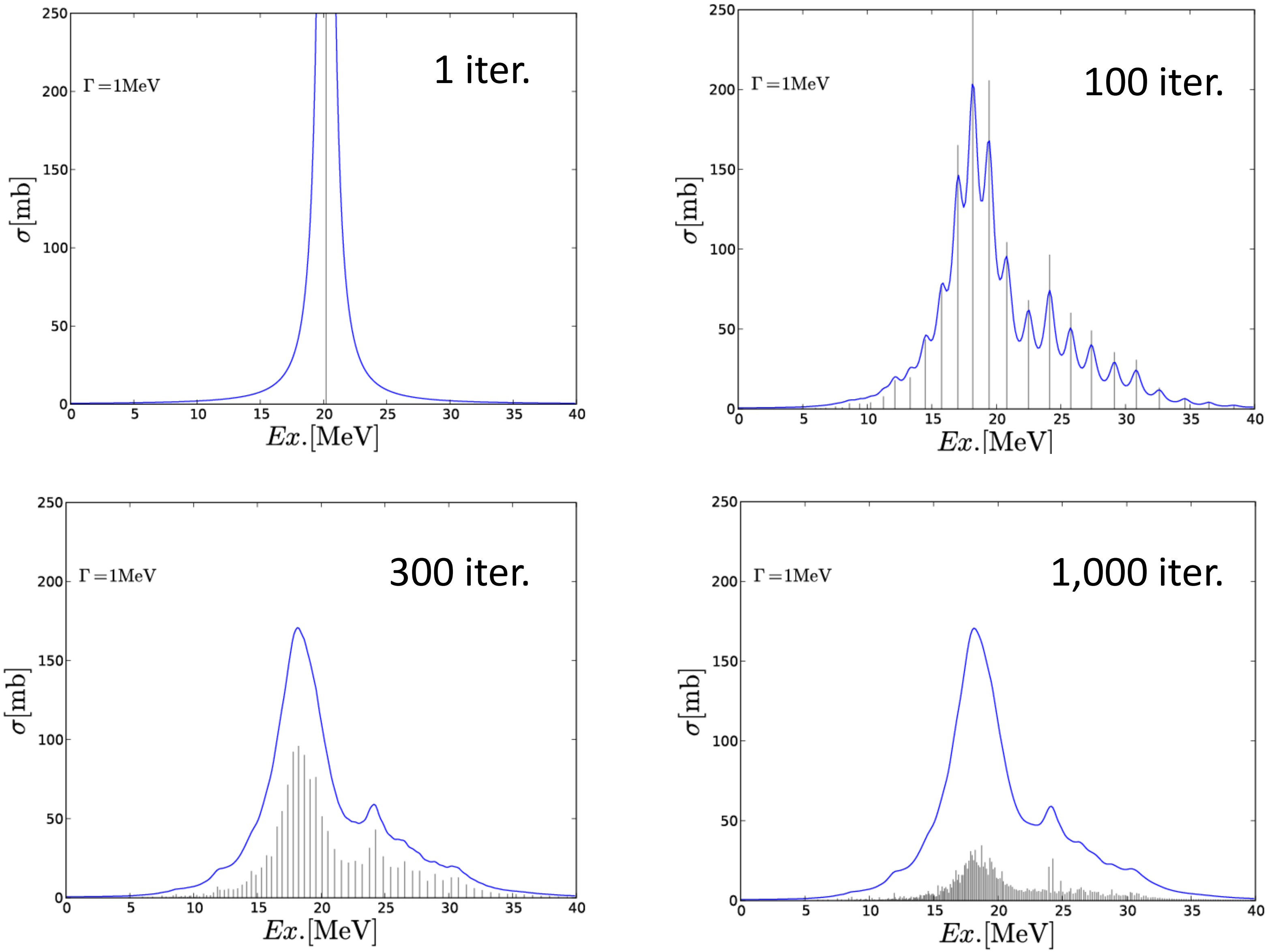

Comparison with exact diagonalization

Exact lowest 3,000 states

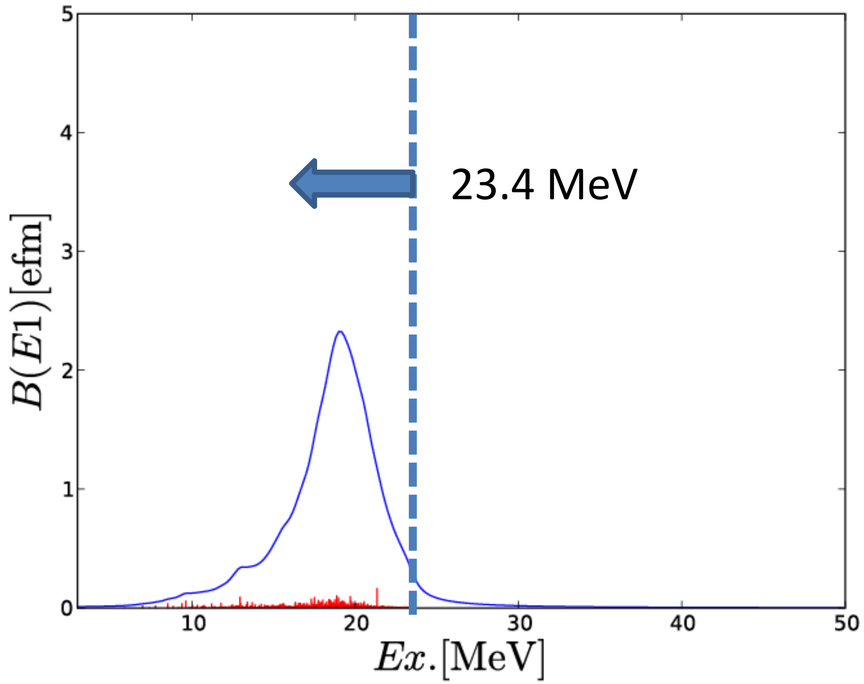

Lanczos strength function (300 iter.)

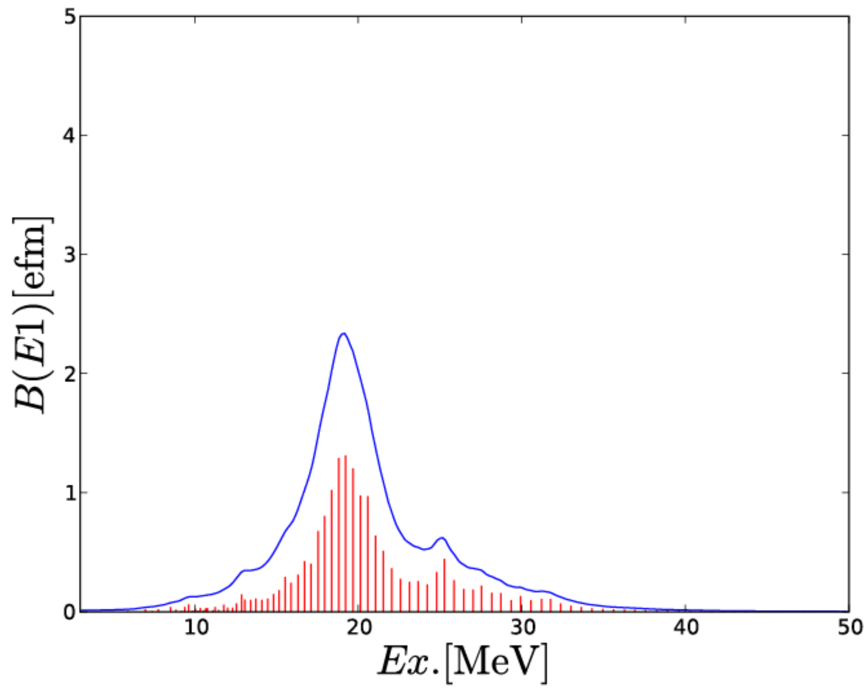

- Smoothing width: Γ=1 MeV
- No visible difference between the two methods

Comparison with experiment for ^{48}Ca

GDR with Γ=1 MeV

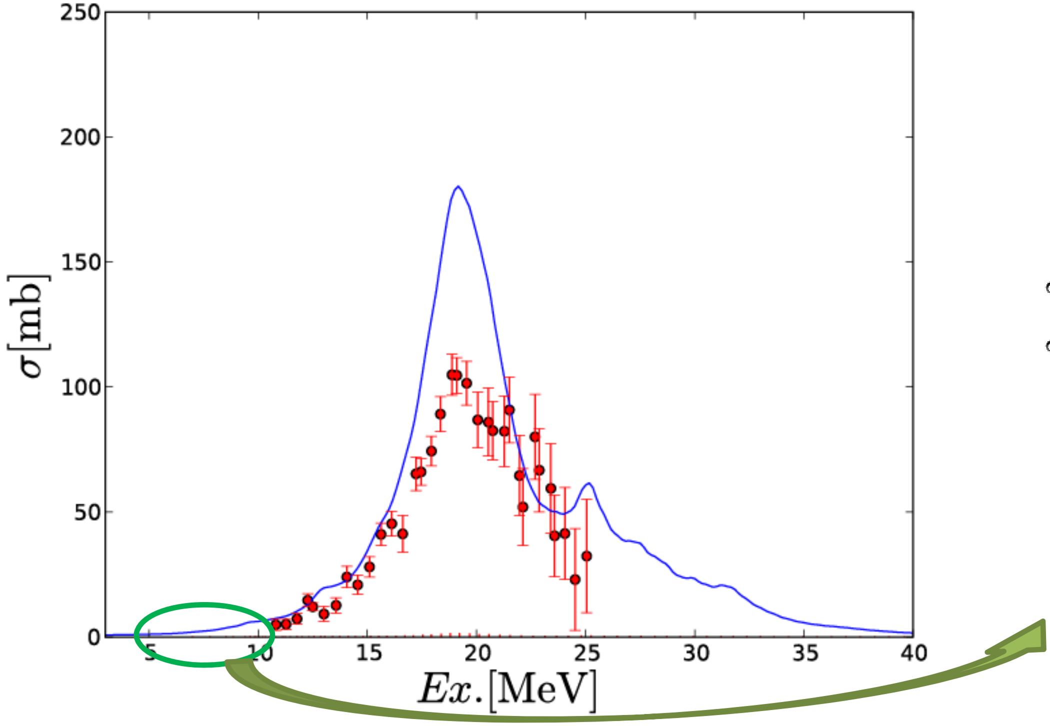

Low-lying 1$^-$ states

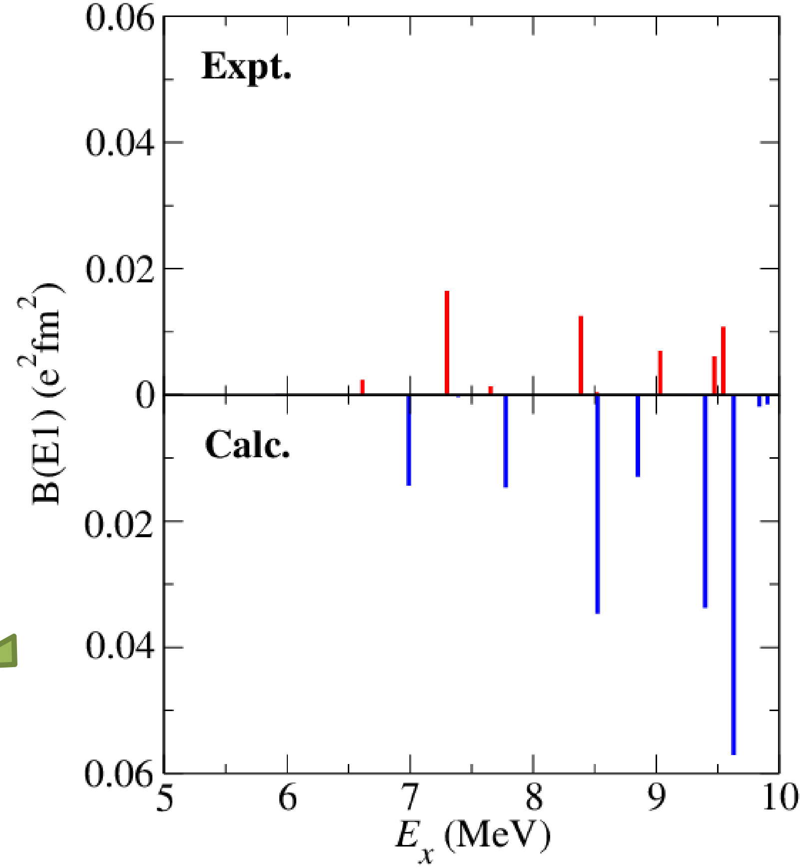

- GDR peak position: good
- GDR peak height: overestimated
- Low-lying states: about 0.7 MeV shifted

need for 2$\hbar\omega$ (g.s.) and 3$\hbar\omega$ (1$^-$)?

Beyond $1\hbar\omega$ calculation

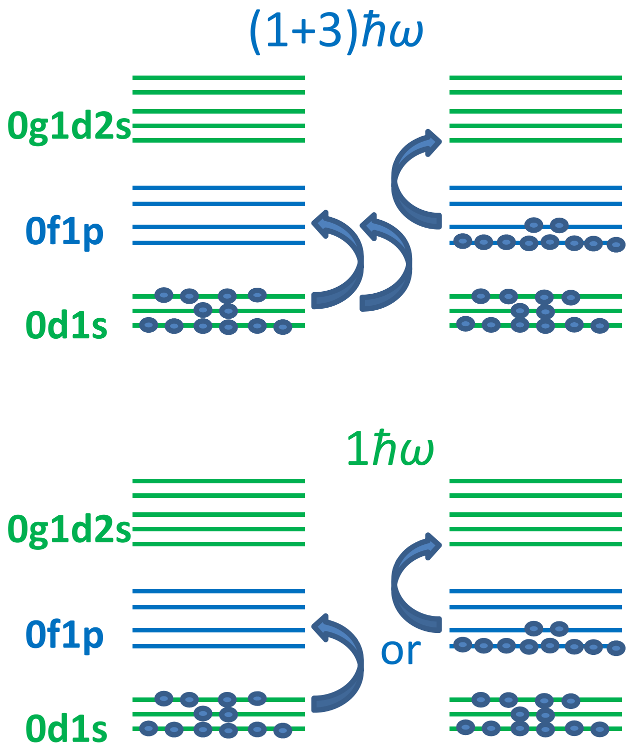

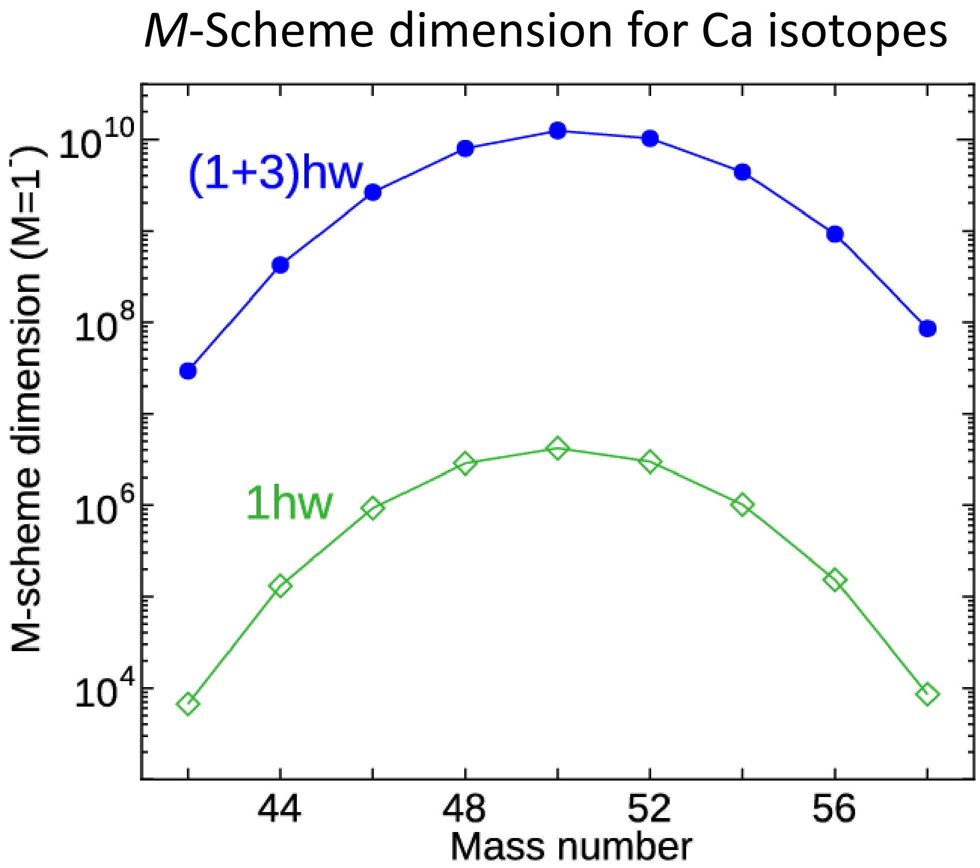

- $3\hbar\omega$ states in the *sd-pf-sdg* shell are included.
  - No single-nucleon excitation to the $3\hbar\omega$ above shell
- Dimension becomes terrible!

KSHELL: MPI + OpenMP hybrid code

N. Shimizu, arXiv:1310.5431 [nucl-th]

- *M*-scheme code
  - "On the fly": Matrix elements are not stored in memory (analogous to ANTOINE and MSHELL64)
- Good parallel efficiency
  - Owing to categorizing basis states into "partition", which stands for a set of basis states with the same sub-shell occupancies

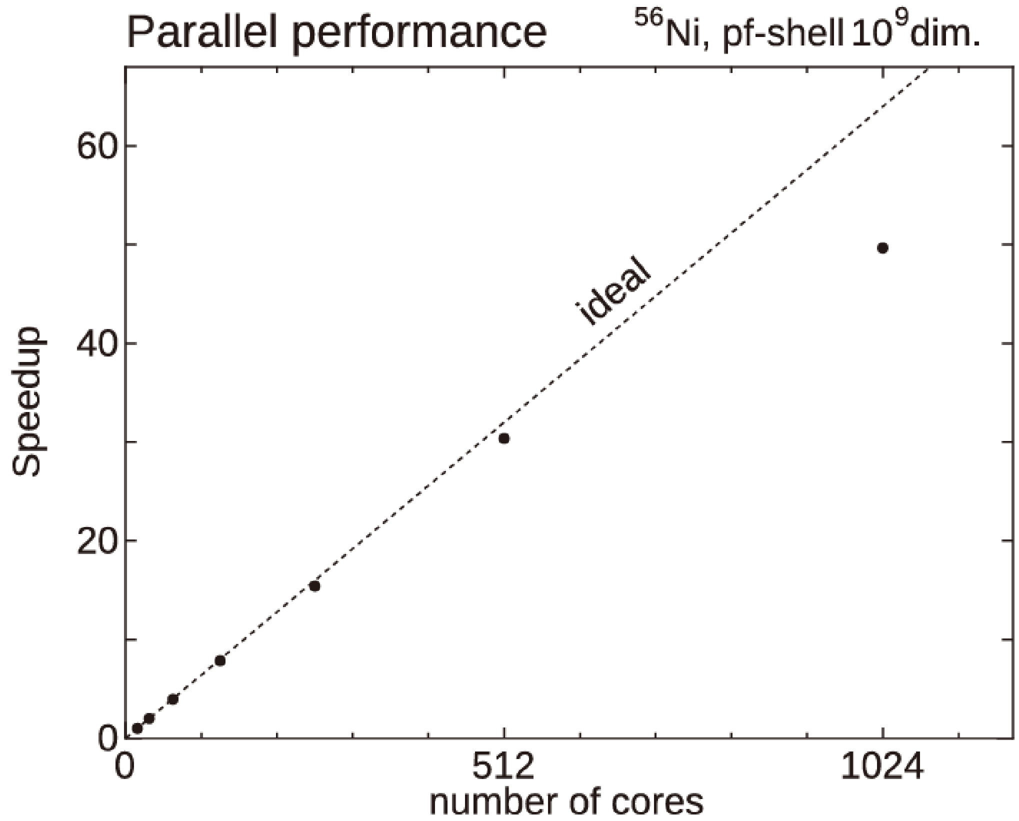

time/iteration : 25 min. (16 cores) ➡ 30 sec. (1024 cores)

Removal of spurious center-of-mass motion

- Usual prescription of Lawson and Gloeckner

  $H' = H + \beta H_{CM}$ with $\beta = 10\hbar\omega/A$ MeV

  – Confirming that eigenstates are well separated

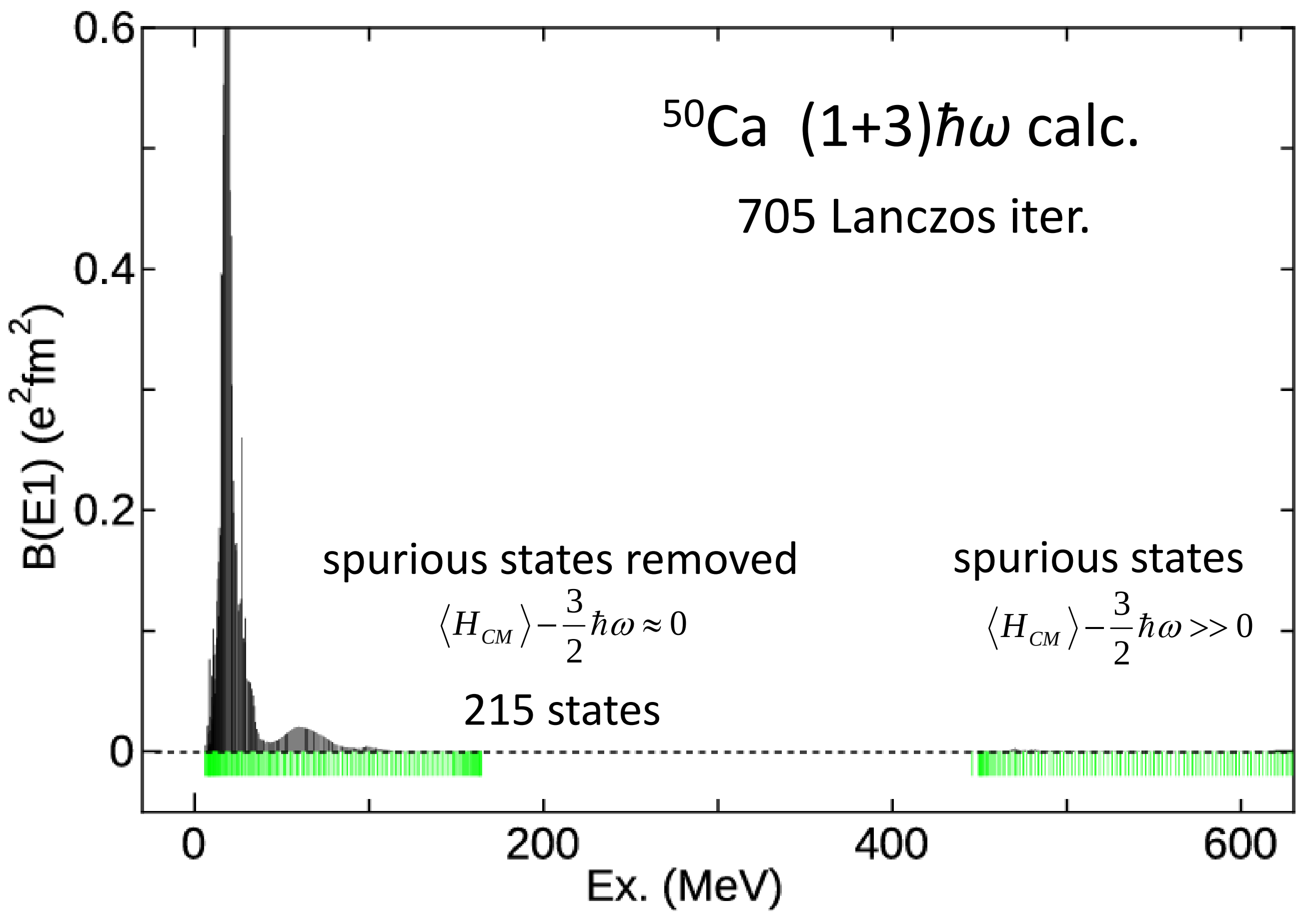

Effect of larger model space

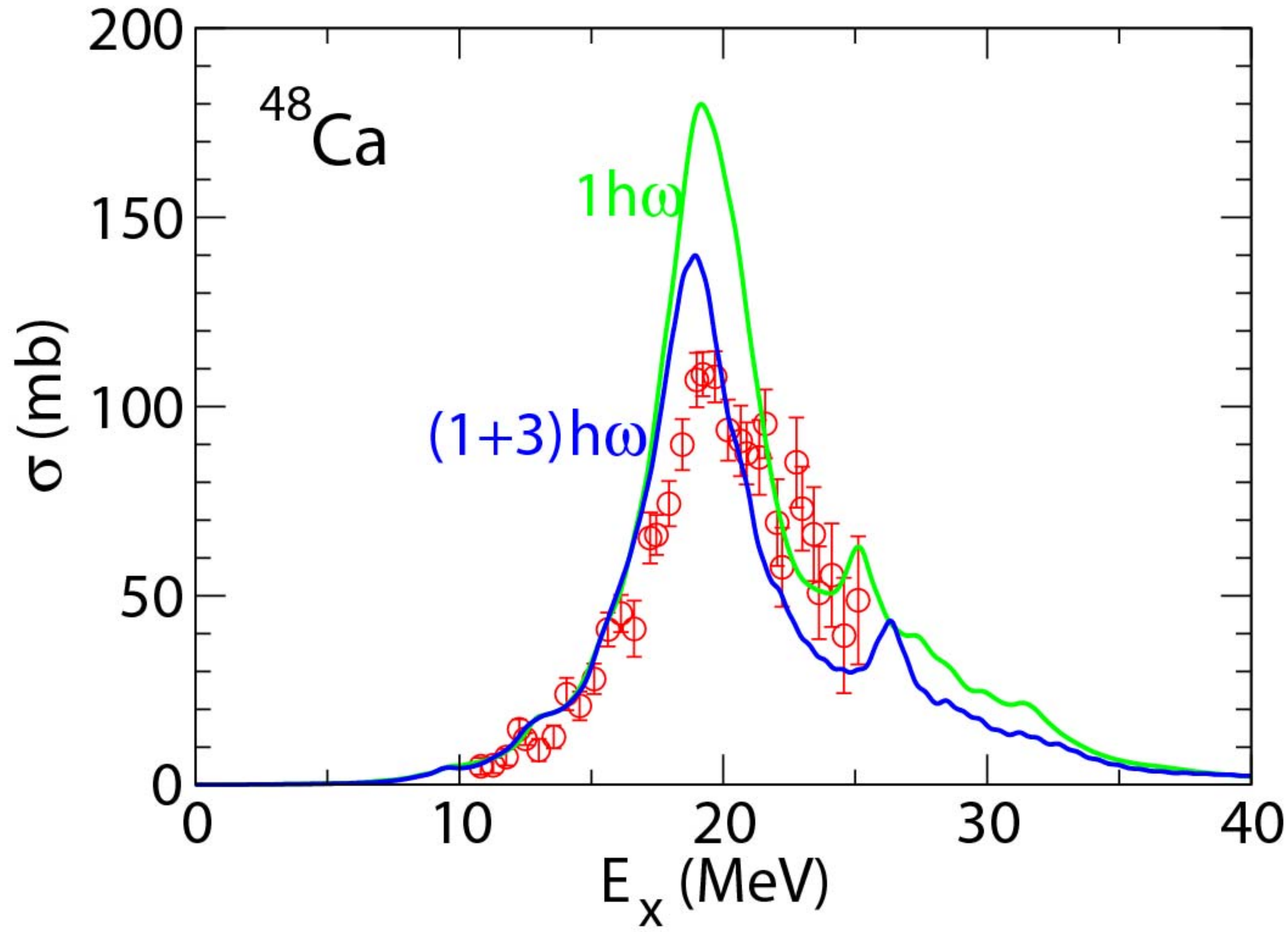

- GDR peak height is improved.
- Low-energy tail is almost unchanged.

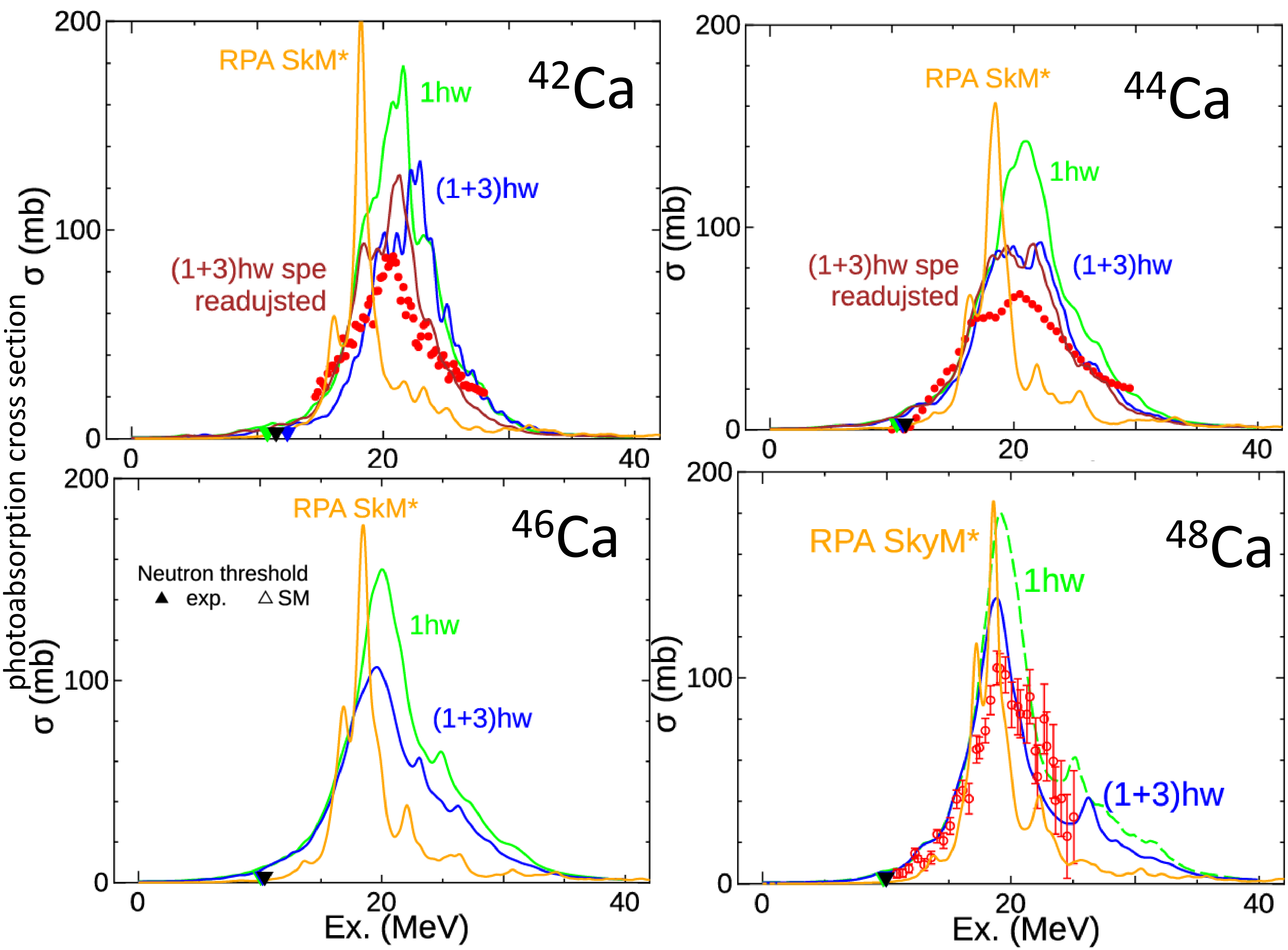

photoabsorption cross section σ (mb)
RPA SkM*
1hw
^{42}Ca
(1+3)hw
(1+3)hw spe
readujsted
RPA SkM*
^{44}Ca
1hw
(1+3)hw spe
readujsted
(1+3)hw
RPA SkM*
^{46}Ca
Neutron threshold
▲ exp. △ SM
1hw
(1+3)hw
RPA SkyM*
^{48}Ca
1hw
(1+3)hw
σ (mb)
Ex. (MeV)
Ex. (MeV)

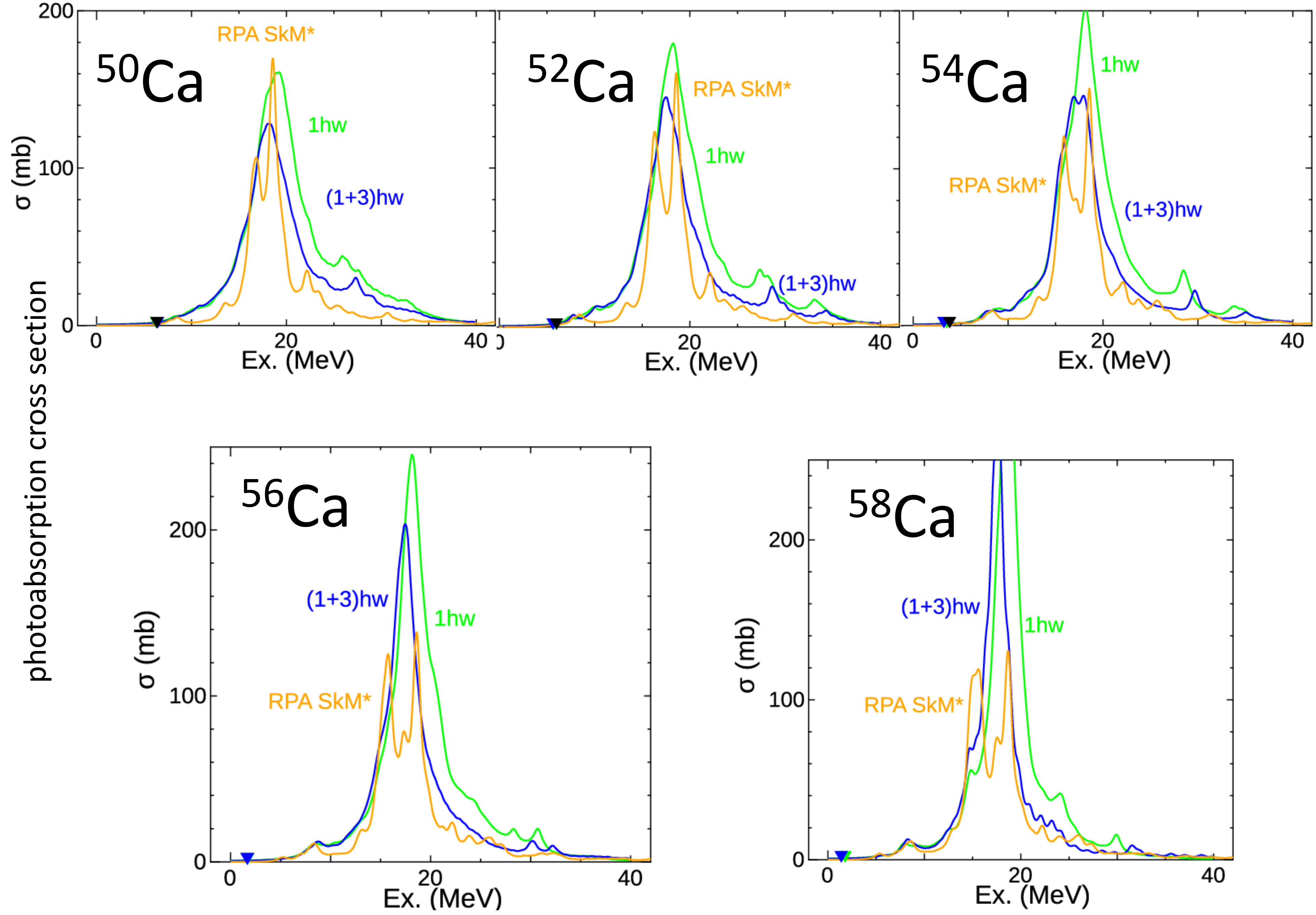

photoabsorption cross section
σ (mb)
Ex. (MeV)
50Ca
52Ca
54Ca
56Ca
58Ca
RPA SkM*
1hw
(1+3)hw

Development of pygmy dipole resonance

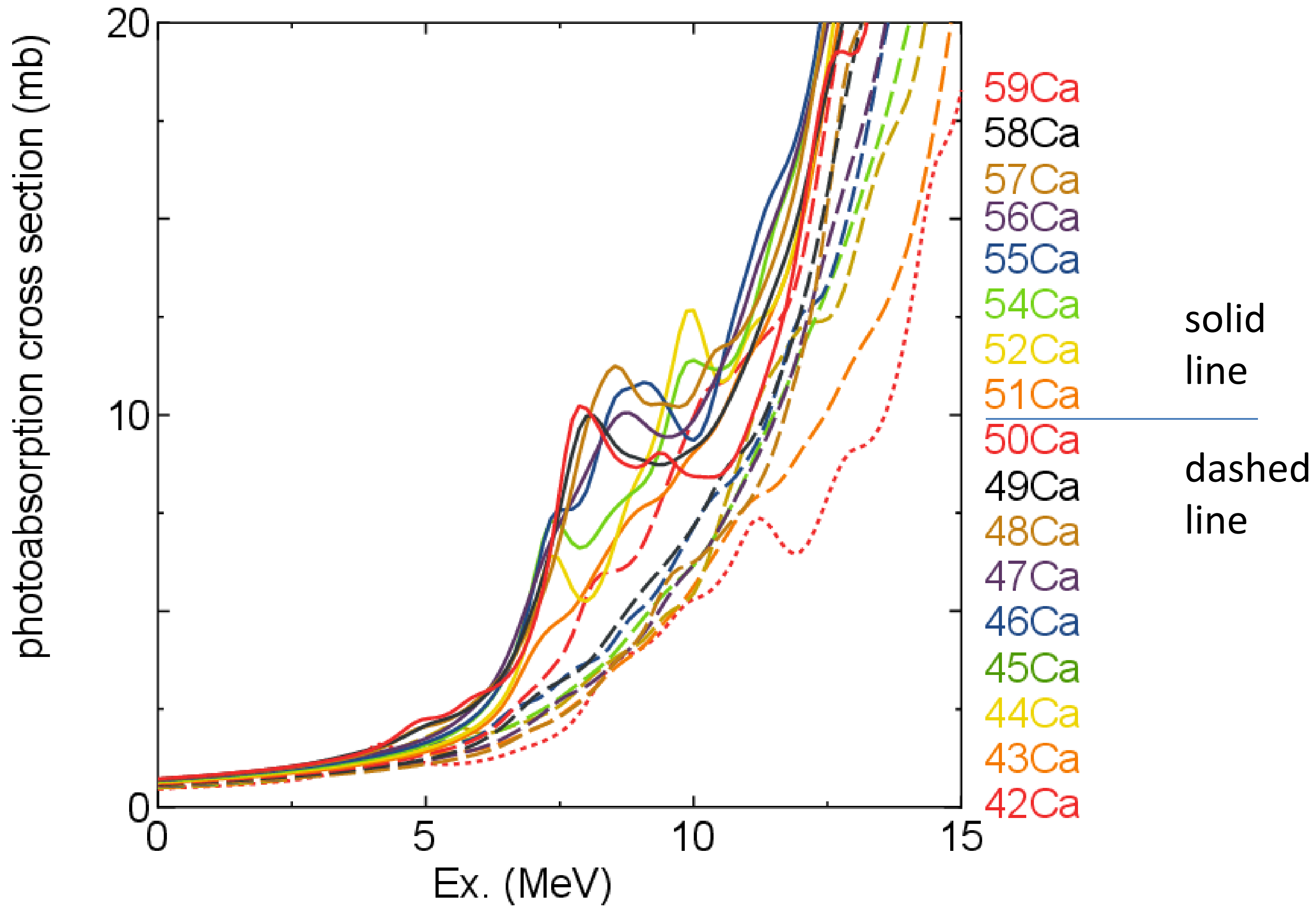

- PDR develops for $A \geq 50$, but the tail of GDR makes the peak less pronounced.

Analyzing SM w.f. in terms of mean-field

Y. Utsuno et al., Phys. Rev. Lett. 114, 032501 (2015).

- Motivated by a recent experiment on ^{44}S
  - Very hindered $E2$ transition from the 4^+_1 to the 2^+_1 state.
  - Shell-model calculation using the SDPF-U interaction "predicts" this property.
- What is the origin of this exotic behavior?
  - Comprehensive description is desired.

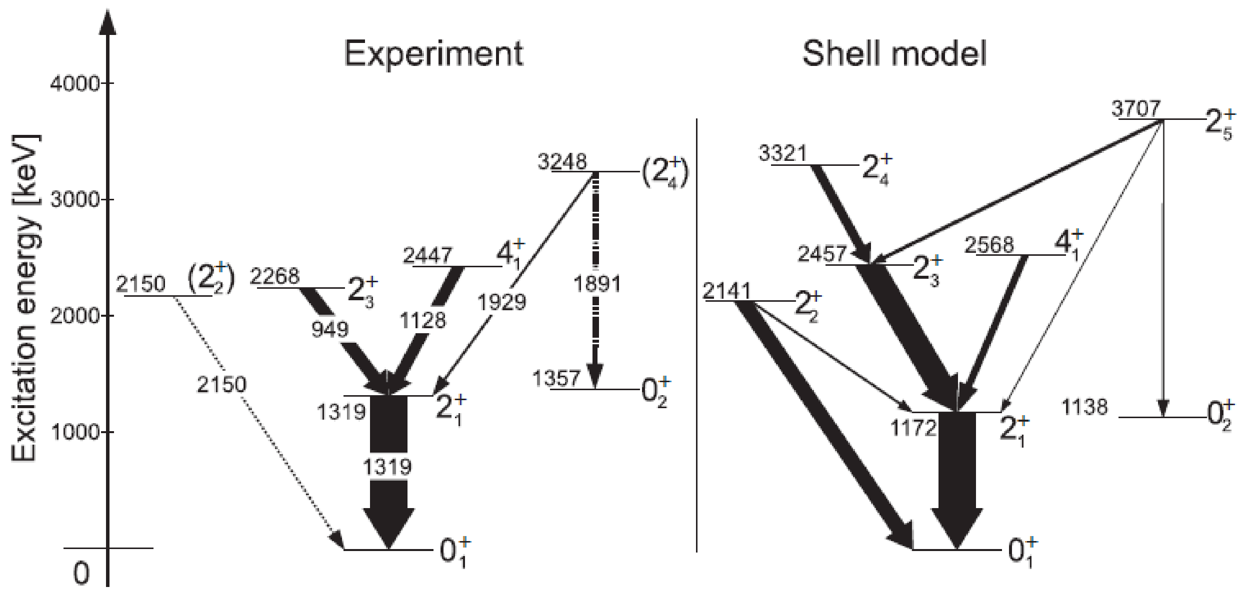

D. Santiago-Gonzalez et al., Phys. Rev. C 83, 061305(R) (2011).

Variation after angular-momentum projection

- Optimize the energy $E^{\mathrm{AMVAP}} = \langle \Psi^{IM} | H | \Psi^{IM} \rangle / \langle \Psi^{IM} | \Psi^{IM} \rangle$ within the angular-momentum projected Slater determinant $|\Psi^{IM}\rangle = \sum_K g_K \hat{P}^I_{MK} |\Phi\rangle$ with $|\Phi\rangle = {a_1}^\dagger \cdots {a_n}^\dagger |0\rangle$ and ${a_k}^\dagger = \sum_l D_{lk} {c_l}^\dagger$.
  - One-basis limit of MCSM
- Model space and effective interaction
  - SDPF-MU in the π(*sd*)ν(*pf*) shell
- Intrinsic properties of the variation after angular-momentum projected (AM-VAP) wave function
  - Deformation (β, γ): from Q_0 and Q_2 of $|\Phi\rangle$
  - Distribution of K numbers: from g_K

Energy levels

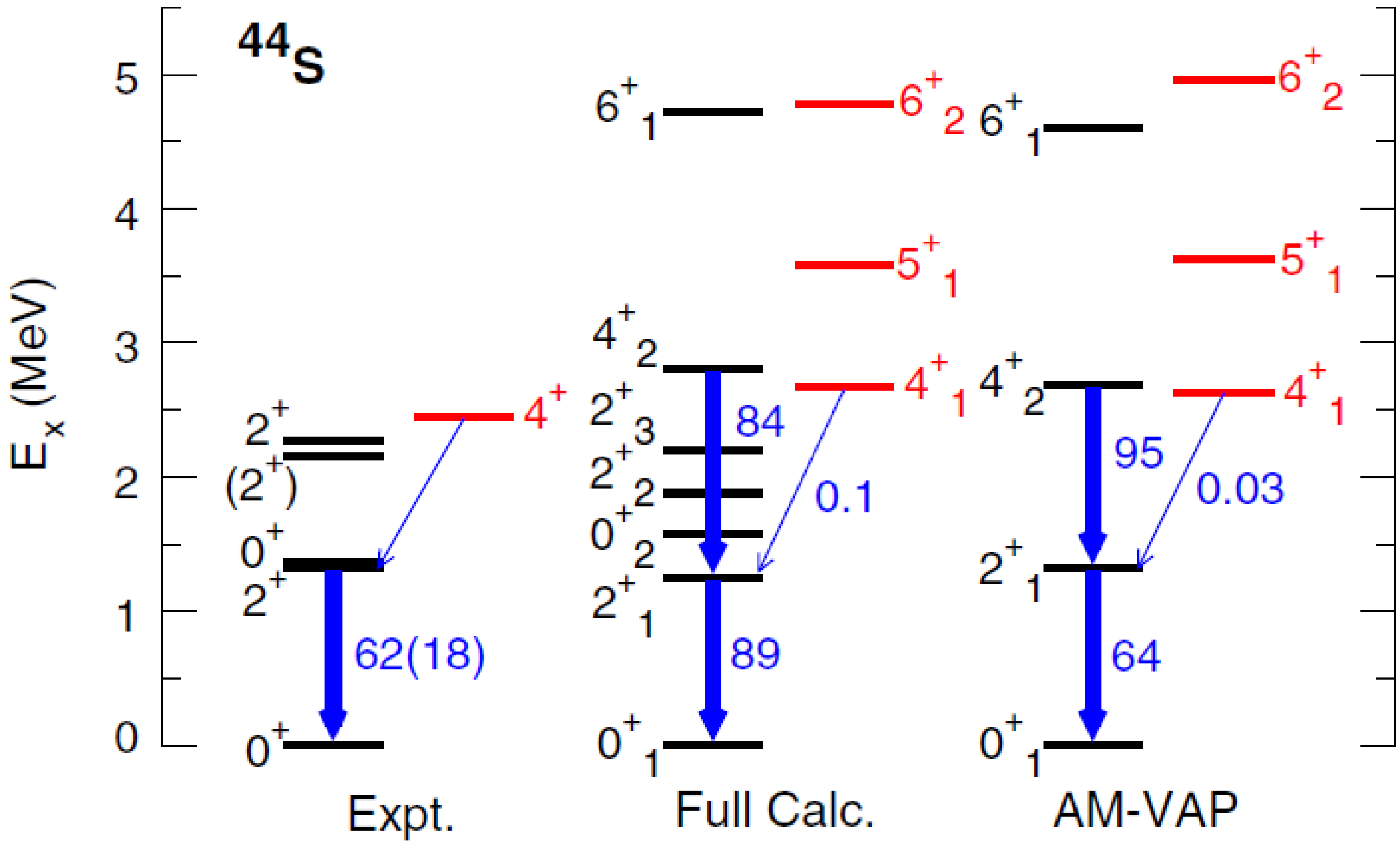

- An isometric 4^+_1 state is obtained both in the SM and the AM-VAP.

Overlap probability between SM and AM-VAP

- $|\langle\Psi(\mathrm{SM})^{IM}|\Psi(\mathrm{AMVAP})^{IM}\rangle|^2$ is a good measure for the quality of AM-VAP states.

$$\langle\Psi(\mathrm{SM})^{IM}|\Psi(\mathrm{AMVAP})^{IM}\rangle$$
$$= \langle\Psi(\mathrm{SM})^{IM}|\sum g_K \hat{P}^I_{MK}|\Phi\rangle$$
$$= \sum g_K^* \langle\Phi\left|\hat{P}^I_{KM}\right|\Psi(\mathrm{SM})^{IM}\rangle^*$$
$$= \sum g_K^* \langle\Phi|\Psi(\mathrm{SM})^{IK}\rangle^*$$

AM-VAP w.f.'s are good approximations to the shell model including 4^+_1.

^{44}S

AM-VAP	SM	Overlap probability
0^+_1	0^+_1	0.915
2^+_1	2^+_1	0.808
3^+_1	3^+_1	0.755
4^+_1	4^+_1	0.859
4^+_2	4^+_2	0.881
5^+_1	5^+_1	0.895
6^+_1	6^+_1	0.545
	6^+_2	0.308
6^+_2	6^+_2	0.538
	6^+_1	0.392

Intrinsic properties in ^{44}S

I^{π}_{σ}	$\lvert K \rvert$							β	γ
	0	1	2	3	4	5	6		
0^+_1	1.00							0.24	33
2^+_1	0.98	0.00	0.01					0.26	23
4^+_2	0.92	0.08	0.00	0.00	0.00			0.28	14
6^+_1	0.76	0.23	0.01	0.00	0.00	0.00	0.00	0.28	13
4^+_1	0.00	0.00	0.00	0.07	0.93			0.23	28
5^+_1	0.00	0.00	0.01	0.08	0.85	0.07		0.23	24
6^+_2	0.00	0.01	0.01	0.14	0.80	0.04	0.00	0.23	26

- *K*=0 and *K*=4 bands
  - *K*=0: usual yrast property; growing *K*=1 with spin due to the Coriolis coupling
  - *K*=4: Concentration of *K* in spite of significant triaxiality
    - Diagonalization in *K* space works.

Why yrast K=4 state?: a hint from ^{43}S

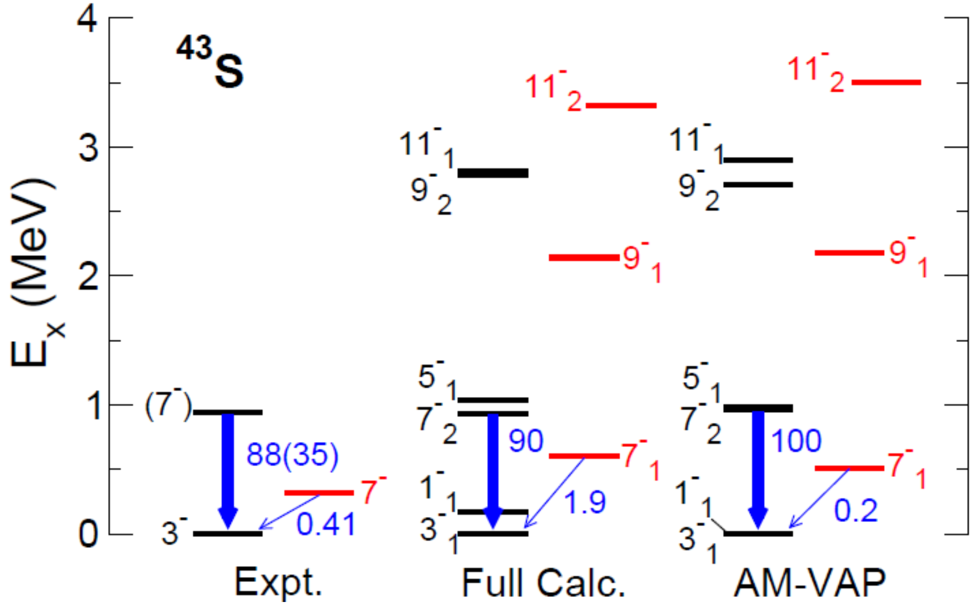

I^π_σ	$\lvert K\rvert$ 1/2	3/2	5/2	7/2	9/2	11/2	β	γ
$1/2^-_1$	1.00						0.27	15
$3/2^-_1$	0.98	0.02					0.25	17
$5/2^-_1$	0.97	0.03	0.00				0.27	16
$7/2^-_2$	0.96	0.04	0.00	0.00			0.25	16
$9/2^-_2$	0.96	0.04	0.00	0.00	0.00		0.28	15
$11/2^-_1$	0.91	0.09	0.00	0.00	0.00	0.00	0.25	16
$7/2^-_1$	0.00	0.01	0.01	0.98			0.22	31
$9/2^-_1$	0.00	0.01	0.04	0.95	0.01		0.23	31
$11/2^-_2$	0.00	0.01	0.01	0.08	0.03	0.87	0.25	37

- Isomeric $7/2^-_1$ state in ^{43}S
  - Reproduced by full calc. and AM-VAP
  - K forbiddeness between K=1/2 and K=7/2 bands
    - Consistent with AMD calc. (Kimura et al., 2013)
    - The band-head energies are very close

Unified understanding of isomerism in sulfur

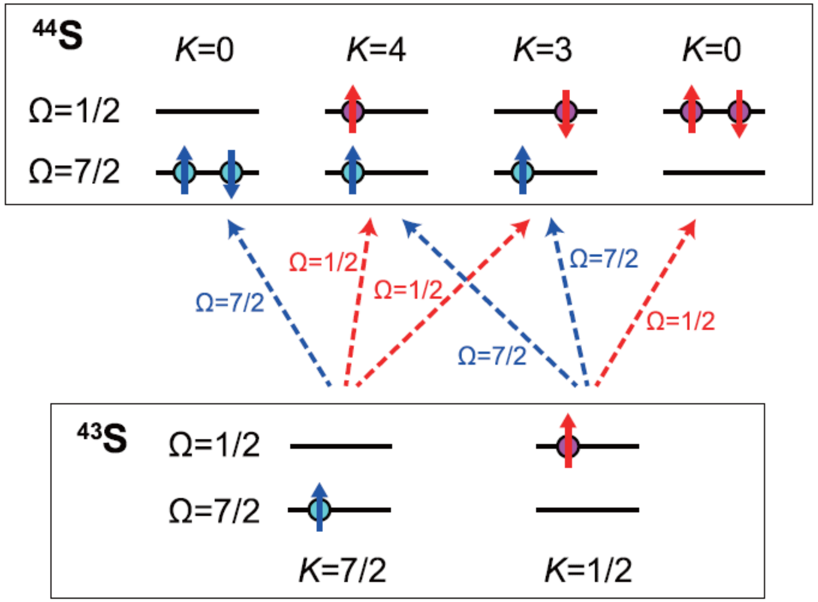

- Two quasiparticle orbits Ω=1/2 and Ω=7/2
  - Located close in energy
- *K*=4: dominated by the two-quasipartcile state Ω=1/2 × Ω=7/2
  - *K*=0 vs. *K*=4 4^+: competition between pairing and rotational energies
    - 2Δ ≈ 2.5 MeV < rotational energy ≈ 3 MeV
- Two *K*=0 states: origin of the very low 0^+_2

Summary

- Shell evolution caused by T=1 cross-shell monopole matrix elements is investigated with large-scale shell-model calculations.
  1. Evolution of the unnatural-parity states of neutron-rich Si
  2. Evolution of the $9/2^+$ states of neutron-rich Cr-Ni isotopes

  Comparison with experiment indicates nearly zero monopole matrix elements, which is consistent with the V_{MU} interaction.
- The evolution of the $g_{9/2}$ orbit in Ca isotopes is discussed.
  – Competition and mixing with core-coupled states
- E1 strength functions in Ca isotopes are calculated.
  – Correlation due to coupling to *p-h* states decreases the total B(E1) values.
- Intrinsic properties of SM w.f. are discussed using variation after angular-momentum projection.
  – Demonstrating a K=4 isomer in ^{44}S